iScience

CellPress
OPEN ACCESS

Article

A modular phage vector platform for targeted photodynamic therapy of Gram-negative bacterial pathogens

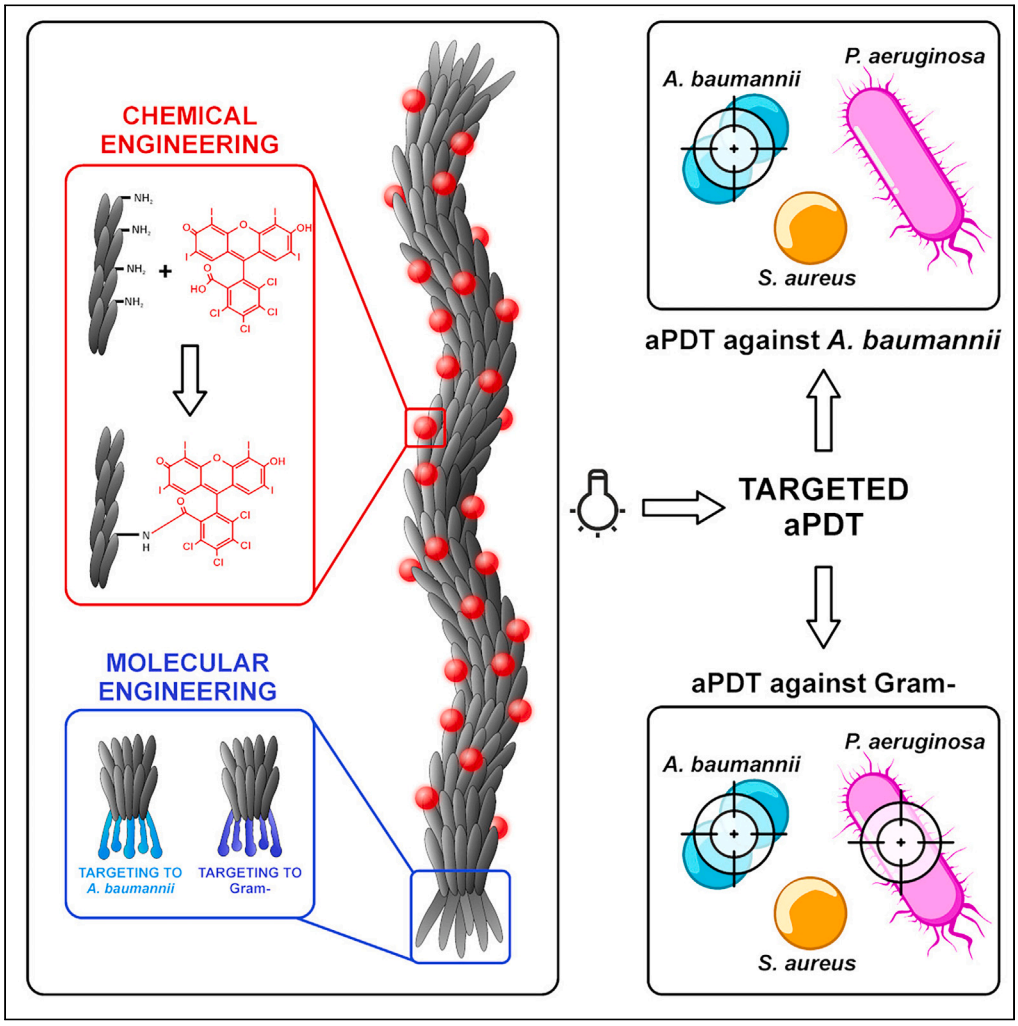

Annapaola Petrosino, Roberto Saporetti, Francesco Starinieri, ..., Paolo Emidio Costantini, Matteo Calvaresi, Alberto Danielli

paolo.costantini4@unibo.it (P.E.C.)
matteo.calvaresi3@unibo.it (M.C.)
alberto.danielli@unibo.it (A.D.)

Highlights

Novel antimicrobial approach based on triggerable nanobiotherapeutics

Antimicrobial photodynamic therapy (PDT) mediated by engineered phage vectors

M13 phages engineered to target specifically diverse Gram-negative bacteria in PDT

Lethal photosensitization of specific targets only upon light irradiation

Petrosino et al., iScience *26*, 108032
October 20, 2023
https://doi.org/10.1016/j.isci.2023.108032

iScience

CellPress
OPEN ACCESS

Article

A modular phage vector platform for targeted photodynamic therapy of Gram-negative bacterial pathogens

Annapaola Petrosino,[1,8] Roberto Saporetti,[2,8] Francesco Starinieri,[1] Edoardo Sarti,[1] Luca Ulfo,[1] Luca Boselli,[3] Andrea Cantelli,[6,7] Andrea Morini,[1] Suleman Khan Zadran,[1] Giampaolo Zuccheri,[1,5] Zeno Pasquini,[4] Matteo Di Giosia,[2] Luca Prodi,[2,5] Pier Paolo Pompa,[3] Paolo Emidio Costantini,[1,*] Matteo Calvaresi,[2,5,*] and Alberto Danielli[1,5,9,*]

SUMMARY

Growing antibiotic resistance has encouraged the revival of phage-inspired antimicrobial approaches. On the other hand, photodynamic therapy (PDT) is considered a very promising research domain for the protection against infectious diseases. Yet, very few efforts have been made to combine the advantages of both approaches in a modular, retargetable platform. Here, we foster the M13 bacteriophage as a multifunctional scaffold, enabling the selective photodynamic killing of bacteria. We took advantage of the well-defined molecular biology of M13 to functionalize its capsid with hundreds of photo-activable Rose Bengal sensitizers and contemporarily target this light-triggerable nanobot to specific bacterial species by phage display of peptide targeting moieties fused to the minor coat protein pIII of the phage. Upon light irradiation of the specimen, the targeted killing of diverse Gram(−) pathogens occurred at subnanomolar concentrations of the phage vector. Our findings contribute to the development of antimicrobials based on targeted and triggerable phage-based nanobiotherapeutics.

INTRODUCTION

The incessant increase in bacterial antibiotic resistance, together with the shortening of new alternatives in the pharma R&D pipelines, has revived interest in phage-inspired antimicrobial approaches against WHO priority I and II pathogens, including many Gram(−) bacteria. Classic phage therapy, envisaging the use of natural lytic phages to control bacterial infections, provides an interesting and useful tool for the control of antibiotic-resistant infections (recently reviewed in[1]), and reports from the majority of studies on their application to treat infections by *Staphylococcus aureus*, *Enterococcus faecium*, *Klebsiella pneumoniae*, *Acinetobacter baumannii*, *Pseudomonas aeruginosa*, *Enterobacter* spp., and *Escherichia coli*—all belonging to the ESKAPEE group of pathogens—are encouraging to date.[2–5] As an alternative to classical approach, the combination of phage therapy with antibiotics administration has been shown to enhance the antimicrobial activity exerted on bacterial infections of various pathogens.[5–7]

However, despite the recent and past successes, classic phage therapy is hampered by several drawbacks, including a generally narrow host range, which needs to be tackled by strain- and patient-tailored precision approaches.[4] Moreover, the likelihood of rapid appearance and spreading of resistance against phage infection and propagation is quite high.[8] An alternative approach is to take advantage of the well-defined molecular biology of several simple model phages (e.g., M13, fd, MS2) for the assembly of genetically retargeted nanobioscaffolds, overcoming the narrow host range of natural phages. These vectors may be armed with (triggerable) antimicrobial functions, providing a modular platform for the treatment of difficult-to-treat infections.[9,10]

Photodynamic therapy (PDT) is likewise considered a very promising therapeutic modality for the eradication of drug-resistant bacteria.[11] PDT is approved for the clinical treatment of several types of diseases, including cancer,[12,13] dermatological pathologies, and microbial infections.[14,15] In PDT, a compound with photosensitizing properties (sensitizer) is accumulated in, or concentrated at, the target cells. The

[1]Dipartimento di Farmacia e Biotecnologie (FaBiT) – Alma Mater Studiorum - Università di Bologna, Via Francesco Selmi 3, 40126 Bologna, Italy
[2]Dipartimento di Chimica "Giacomo Ciamician" – Alma Mater Studiorum - Università di Bologna, Via Francesco Selmi 2, 40126 Bologna, Italy
[3]Nanobiointeractions and Nanodiagnostics Laboratory, Istituto Italiano di Tecnologia (IIT), Via Morego 30, 16163 Genova, Italy
[4]Infectious Diseases Unit, IRCCS Azienda Ospedaliero-Universitaria di Bologna, Italy
[5]CIRI SDV – Centro Interdipartimentale Scienze della Vita - Alma Mater Studiorum - Università di Bologna, Via Tolara di Sopra, 41/E - 40064 Ozzano dell'Emilia (BO), Italy
[6]CNR Institute of Molecular Genetics "Luigi Luca Cavalli-Sforza" Unit of Bologna, Italy
[7]IRCCS Istituto Ortopedico Rizzoli, Bologna, Italy
[8]These authors contributed equally
[9]Lead contact
*Correspondence: paolo.costantini4@unibo.it (P.E.C.), matteo.calvaresi3@unibo.it (M.C.), alberto.danielli@unibo.it (A.D.)
https://doi.org/10.1016/j.isci.2023.108032

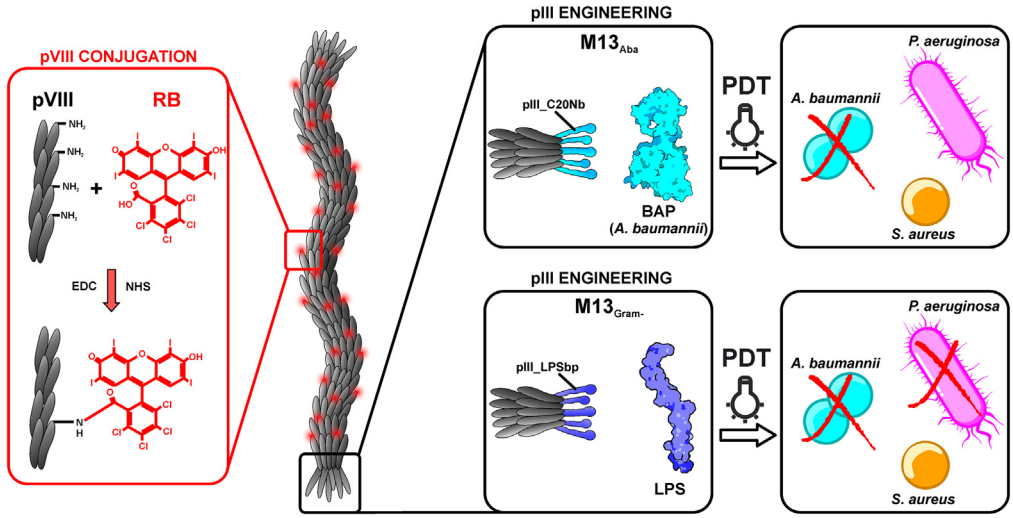

Figure 1. Orthogonal engineering of M13 phage for selective PDT

Phages with targeted tropism against *Acinetobacter baumannii* (light blue) and against the gram-negative *Acinetobacter baumannii* and *Pseudomonas aeruginosa* cells (dark blue) were generated. $M13_{Aba}$ is retargeted to the biofilm activating protein (BAP) of *Acinetobacter baumannii* through the specific display on the minor coat protein pIII of the C20 nanobody (C20Nb), whereas $M13_{Gram-}$ targets the lipopolysaccharides of the Gram-negative outer membrane through the display on the pIII protein of KNYSSSISSIRAC-binding peptide (LPSbp). The amino group of $M13_{Aba}$ and $M13_{Gram-}$ major capsid protein pVIII were chemically conjugated with hundreds of RB for the production of ROS, which are highly antimicrobial, upon light irradiation, in the cell proximity.

subsequent triggering of the sensitizer by light generates highly reactive oxygen species (ROS), whose local burst exerts lethal effects on the target cancer or microbial cells.[15] Antimicrobial photodynamic therapy (aPDT) already finds a wide use for topical, dental, and soft tissue infections, either alone or in combination with photosensitizers.[16–19] Moreover, aPDT can stimulate the immune system to improve bacterial clearance.[20] The combination of antibiotic therapy with PDT has also been proven efficient in eliminating drug-resistant bacteria in patients carrying microflora resistant to a previous antibiotic therapy,[21,22] whereas studies on animals have reported little evidence of host tissue damage following aPDT.[17,23]

Compared with conventional antibiotic therapies, antimicrobial PDT presents several interesting assets: (1) the burst of ROS affects multiple biological informational molecules at once (e.g., DNA, RNA, proteins, lipids, etc.) and disrupts membrane integrity, thus providing physical damage to cells, which less likely engenders resistance; (2) PDT is also effective, for the same reasons, on metabolically inactive, dormant, and antibiotic-resistant cells; (3) PDT can be applied locally, exploiting the possibility to focus the triggering irradiation at the desired site of action; and (4) it presents an instant onset of action.

However, a major limitation of photodynamic (as well as sonodynamic and photothermal) antimicrobial agents is that the reactive oxygen species (or the heat) generated during irradiation can harm bystander host cells. Accordingly, there is extraordinary interest in developing methods for specifically targeting the sensitizers to the infectious organism.[24] The advantage of targeting the photosensitizer is that ROS production is generated only in immediate proximity of the pathogen, allowing for lower irradiation and sensitizer dosages needed to achieve lethal photosensitization. Several studies have shown the effectiveness and reduced toxicity of PDT, in conjunction with sensitizer targeting systems, including proteins (ConcanvalinA-RB[25]), antibodies, chemical modification, or nanoarchitectonics of vector particles[24,26–30] and phages.[31]

Owing to the distinct cell surfaces, aPDT can have very different effects on Gram-positive and Gram-negative bacteria. PSs can penetrate through the cell walls of Gram-positive bacteria with higher ease, whereas Gram-negative bacteria display various degrees of resistance to PS permeabilization, due to the presence of the outer membrane, acting as a barrier to diverse drug molecules.[32] To solve this problem, outer-membrane-disrupting agents or the chemical manipulation of bacterial surface structures has been proposed.[33] Nevertheless, such pre-treatments may be accompanied by potential cytotoxicity of the agents used.

Despite the respective advantages provided by phage-derived therapies and PDT, only a handful of phage applications for antimicrobial PDT have been reported to date, principally involving the use of natural phages decorated with chlorine e6.[34] Moreover, a systematic retargeting of photosensitizer-decorated phages through specific bacteria-targeting moieties (antibodies and peptides) has never been reported, except for one study in which chimeric M13 phages were conjugated to gold nanoparticles for antimicrobial photothermal therapy.[35] This leaves a wide avenue open for scientific discovery and methodological improvements.

Filamentous bacteriophages such as M13 represent a harmless and effective delivery platform. They can undergo extremely flexible genetic engineering, allowing for a plethora of targeting designs.[9] M13 can provide high avidity for the target due to its multivalent display of specific targeting moieties and a multitude of functionalization sites resulting in a high payload of effectors.[36] In particular, the possibility to conjugate M13 with hundreds of photosensitizers[37–39] makes them interesting vectors for antimicrobial PDT applications (Figure 1).

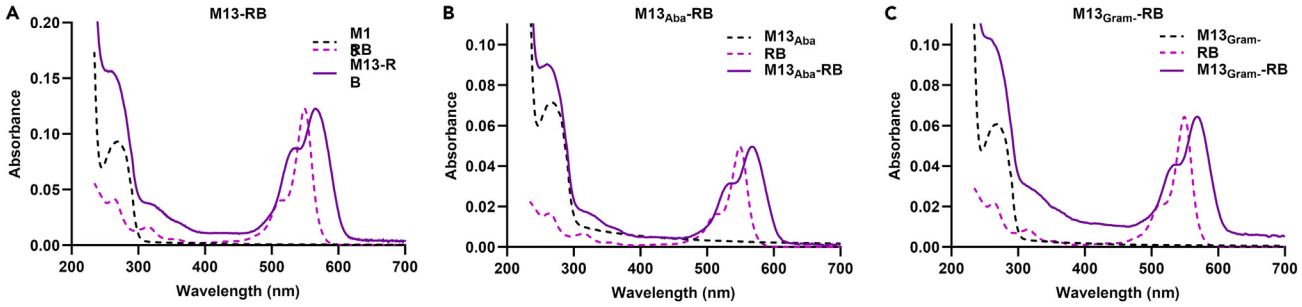

Figure 2. Conjugation of RB to M13 phage

(A–C) Chemical conjugation was performed on (A) M13, (B) $M13_{Aba}$, and (C) $M13_{Gram-}$ phages. Absorption spectra of phages (dashed black line), RB (dashed pink line), and phage conjugated with RB (purple line).

Here we present a flexible and robust M13-based platform for antimicrobial PDT against Gram(−) bacterial pathogens. M13 phages with specific tropism against *A. baumannii* were generated by phage display of a specific nanobody (C20) on the minor coat protein g3p. Likewise, the fusion of an LPS-binding peptide to g3p enabled to expand the target range to different Gram(−) pathogens, not targeted by wild-type M13. These engineered vectors were orthogonally functionalized with hundreds of Rose Bengal (RB) sensitizers on the major capsid protein g8p, generating nanobioconjugates able to selectively kill their specific targets only upon light irradiation. RB was chosen as it is a widely available and biocompatible photoreactive fluorescein derivative, approved by the FDA as an ocular diagnostic stain and orphan anticancer drug.[40] RB contains multiple halogens (i.e., chlorine, iodine) with high atomic number substituents, which enhance the intersystem crossing rate, generating a triplet excited state underlying effective generation of ROS.[25,40] Following RB conjugation, the M13-RB phage nanobioconjugates were shown to promote photodynamic generation of ROS and mediate selective killing of their specific targets only upon light irradiation.

RESULTS

Conjugation of Rose Bengal to the capsomers of M13 produces an ROS-generating phage PDT platform

To prove that M13 can be engineered into a valuable vector platform for PDT applications, we set out to conjugate RB to the capsomers of the M13K07 phage (hereafter referred to as M13). A shifted and broader peak at 560 nm in the absorption spectrum was observed following conjugation with M13 (Figure 2). These spectral changes confirmed that RB was covalently linked to the M13 capsid.[41] Considering the initial M13 concentration and the molar extinction coefficients of RB, 971, 405, and 562 RB molecules were attached to M13, $M13_{Aba}$, and $M13_{Gram-}$, respectively (Table 1).

Specific photokilling of the natural *E. coli* host by a wild-type M13-RB bioconjugate

Next, the M13-RB conjugates were tested for their photodynamic antimicrobial activity on *E. coli* TG1 and two other Gram-negative bacteria, *P. aeruginosa* PA14 and *A. baumannii* ATCC 19606 (Aba). TG1 is a natural host for M13, expressing the F′ pilus, representing the primary receptor bound by the wild-type g3p phage protein promoting infection. On the contrary, *P. aeruginosa* and *A. baumannii* lack the F′ pilus and are not efficiently targeted by wild-type M13.[42] Free Rose Bengal was used as control to benchmark phage-mediated PDT against the non-targeted approach. All bacterial strains tested exhibited variable sensitivity to the photodynamic treatment, presumably due to biochemical, metabolic, or genetic differences (Figure 3). In particular, *E. coli* TG1 viability was only partly (13.6% $\pm$ 12.3%) affected after incubation with 1 μM free RB equivalents, whereas *P. aeruginosa* PA14 suffered extensive (42.8% $\pm$ 6.6%) killing under the same conditions. Finally, after irradiation, *A. baumannii* proved to be the least sensitive to free RB, remaining essentially unaffected by PDT with 1 μM free RB. Despite these differences, M13-mediated photodynamic treatment increased the killing only toward the TG1 host strain, starting at 100 nM RB equivalents (Figure 3A). Stronger, dose-dependent photodynamic effects were recorded at the highest sensitizer concentration tested (1 μM), where the M13-RB platform increased PDT killing of TG1 cells by more than five orders of magnitude with respect to free RB alone. Remarkably, the M13-RB vector was not able to induce a significant increase in mortality (compared with free RB) on Aba and PA14. The lack of specificity toward these strains indicates that wild-type M13 can prime the accumulation of sufficient RB photosensitizers only toward its natural host, expressing the F′ pilus. These results show that the M13 phage is an excellent platform for implementing selective antimicrobial PDT.

Retargeting of M13 against *Acinetobacter baumannii*

To investigate whether the phage PDT platform could be engineered to target different bacteria from the native *E. coli* F+ host strains, M13 was retargeted to bind to *A. baumannii* cells. The coding sequence of the C20 single domain antibody (sdAb or nanobody) recognizing the *A. baumannii* biofilm-associated protein (BAP) was fused to the C-terminal domain of the pIII (g3p) minor coat protein in the phage. This choice was driven by the high specificity of C20 for *A. baumanni* BAP along with a low cross-reactivity toward other bacterial species.[43]

Table 1. Description and main characteristics of conjugated phages

Name	Targeting moiety	Target	[Phage] (v/mL)	[Phage] (nM)	[RB] (μM)	Ratio (RB/phage)
M13	pIII	F′ pilus of *E. coli*	8.43E+12	14.0	13.6	971
$M13_{Aba}$	C20 nanobody	BAP protein of *A. baumannii*	1.02E+13	17.0	6.89	405
$M13_{Gram-}$	Li005 peptide	LPS of gram-negative bacteria	9.57E+12	15.9	8.94	562

The pPK_C20 phagemid carrying the C20-pIII fusion was co-transformed with the hyperphage plasmid lacking both the native pIII cistron as well as the F1 phage origin. This strategy allowed to voiding the undesired residual packaging of the helper phage, resulting in uniform and stable recombinant virions of about 500 nm length, packaging only the C20-pIII phagemid, as validated by TEM (Figure 4C) and atomic force microscopy (AFM, Figures 4D and 4E). Immunoblotting with a pIII-C-term-specific antibody demonstrated the correct phage display of a 36.9 kDa polypeptide compatible with the expected molecular weight of the C20-pIII (C-term) fusion, absent from the wild-type M13 phages (Figure 4B). This strategy allowed to overcome occasional wild-type pIII recycling from the superinfection of helper phages, resulting in $M13_{Aba}$ virions displaying only the C20-pIII(C-term) fusion.

The specific retargeting of $M13_{Aba}$ to *A. baumannii* was demonstrated by qPCR. *S. aureus* and *P. aeruginosa* were used as negative controls, respectively for Gram(+) and Gram(−) pathogens, as they lack orthologues of the BAP protein recognized by the C20 sdAb fusion. After incubation, washing, and pelleting of the bacteria, the great majority (61.9% ± 16.7%) of $M13_{Aba}$ phages were bound to *A. baumannii* cells, whereas a significantly lower fraction of phages interacted with both *S. aureus* (16.6% ± 1.7%) and *P. aeruginosa* (2.2% ± 2.4% <3%) cells (Figure 4F). Taken together, these results demonstrate that phage display of the C20 sdAb on pIII allows the selective retargeting of M13 to *A. baumannii* cells.

Potent phage-mediated PDT against *Acinetobacter baumannii*

Next, the recombinant $M13_{Aba}$ vector was armed with hundreds of RB molecules taking advantage of the extremely high multiplicity of the pVIII capsomer, providing thousands of amine groups for the chemical conjugation of the RB sensitizer on the vector capsid. After conjugation and removal of unreacted RB, the $M13_{Aba}$-RB vector was tested for the generation of ROS. The ability of phage conjugates to generate ROS, upon irradiation with visible white light, was evaluated using the Amplex Red and ABMDMA assays, respectively, to detect peroxides and $^1O_2$. Results indicated that the conjugation of RB to phage improved the generation of peroxide (8-fold increase) over singlet oxygen production (4-fold decrease, φ_Δ decrease from 0.76 to 0.20) with respect to free RB, suggesting a photoactivation switch favoring type I over type II mechanisms after PS bioconjugation with proteins (Figures 5A and 5B).[44,45] The results clearly showed that M13 virions can be conjugated to several hundreds of RB sensitizer molecules, without quenching the ability to produce cytotoxic ROS, providing a high sensitizer payload.

To exclude impairment of vector targeting after conjugation with the sensitizer, the specificity of $M13_{Aba}$-RB for *A. baumannii* cells was evaluated by flow cytometry, taking advantage of the intrinsic fluorescence of RB. Again, *S. aureus* and *P. aeruginosa* were used as negative controls. As a result, 97.9% of fluorescent events were detected for an *A. baumannii* culture incubated with the $M13_{Aba}$-RB phage conjugate, confirming excellent binding even after conjugation with the photosensitizer. On the contrary, $M13_{Aba}$-RB bound only a minor fraction of *S. aureus* and *P. aeruginosa* cells, confirming the lack of affinity for non-specific targets (Figures 5C and 5D). These results demonstrate that the tropism of M13 can be successfully modified to target a specific bacterial species and that the retargeted M13 virions withhold specificity even after conjugation with hundreds of photosensitizers.

To test the efficacy of the $M13_{Aba}$-RB bioconjugate, antimicrobial PDT assays were performed. Interestingly, the $M13_{Aba}$-RB bioconjugate showed no antimicrobial effects without irradiation, whereas photostimulation of $M13_{Aba}$-RB led to the killing of more than 75% of *A. baumannii* cells at 0.25 μM RB equivalents (Figure 5E). Considering the phage functionalization rate (Table 1), this value corresponds to a

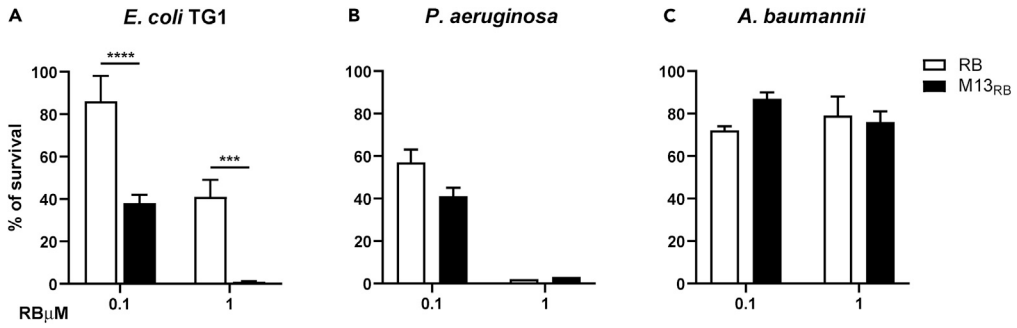

Figure 3. Antimicrobial PDT of M13-RB bioconjugates

(A–C) The survival rate of bacterial cells incubated with increasing concentration of either RB (white bars) or M13-RB (black bars) and irradiated with a white led amp for 45 min. PDT assays were performed on (A) *E. coli*, (B) *P. aeruginosa*, and (C) *A. baumannii*. Data are represented as mean ± SD. *** = $p < 0.001$, **** = $p < 0.0001$.

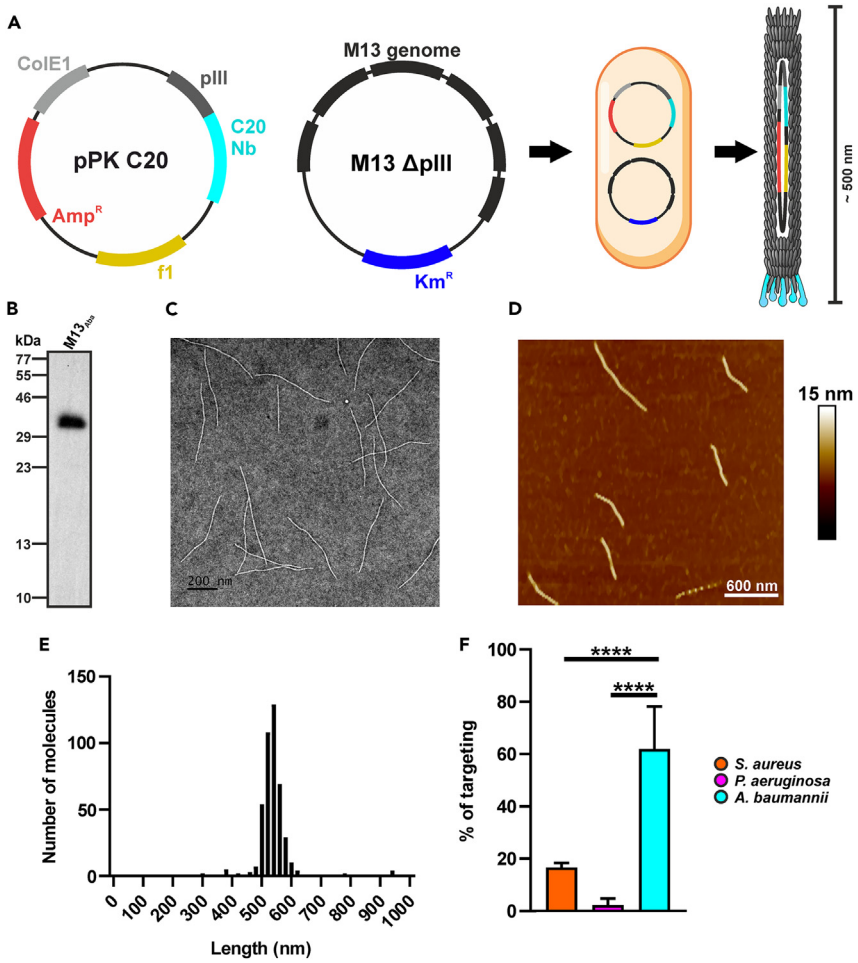

Figure 4. Characterization of the anti-*A. baumannii* phage M13$_{Aba}$

(A) Schematic representation of the M13 genetic engineering through co-transformation in *E. coli* of ppK_C20 phagemid and hyperphage genome.

(B–D) (B) Immunoblotting of the antiBAP_Nb-pIII fusion (M13$_{Aba}$), demonstrating incorporation in the purified virion. The integrity of purified M13$_{Aba}$ phages was visualized through (C) TEM (scale bar = 200 nm) and (D) AFM (scale bar = 600 nm).

(E) M13$_{Aba}$ length distribution analyzed by AFM.

(F) Specificity and selectivity of engineered M13$_{Aba}$ phages targeting *A. baumannii*: the binding was determined by SyberGreen real-time PCR using an oligonucleotide that anneals on the pIII minor-coat-protein-coding gene. M13$_{Aba}$ phages showed significant binding to *A. baumannii* (cyan), whereas poor binding was observed to *S. aureus* (orange) and *P. aeruginosa* (magenta). Data are represented as mean ± SD. **** = $p < 0.0001$.

picomolar (pM) effective vector concentration. The bacterial photokilling proved phage concentration-dependent, as indicated by increased *Acinetobacter* survival rates at 0.1 μM RB equivalents, whereas free RB sensitizer molecules (not conjugated to phage) showed no significant effect at the same concentrations (data not shown). The absence of photodynamic effects was also observed for *S. aureus* and *P. aeruginosa*, proving the specific killing mediated by the engineered phage (Figure 5E). These results demonstrate a potent and light-dependent antimicrobial effect of the engineered M13 platform, only toward the specific target pathogen. To further validate the photodynamic killing of *A. baumannii* and provide first insights into the possible killing activity triggered by the phage vector, live/dead and metabolic assays were carried out. After incubation with the M13$_{Aba}$-RB bioconjugates, *A. baumannii* cells showed a strong light-dependent shift in viability in cytofluorometry: under dark conditions all cells stained positive for SYTO9 only, a hallmark of live cells (Figure 5F). Shortly after irradiation (20 min post-irradiation) a large fraction of the population stained positive for propidium iodide (PI, Fig, 5G), comprehending a minor fraction of injured cells (SYTO9/PI positive) and more than 70% of dead cells (PI positive, SYTO9 negative) (Figure 5H). This result demonstrates that the fast onset of phage-mediated aPDT is accompanied by a rapid permeabilization of the cell membrane, as most of the bacterial population becomes positive to the otherwise non-permeant PI stain. Metabolic assays showed a 70% decrease in the capacity to reduce tetrazolium violet following irradiation (Figure 5I), consistent with the observed decrease in vitality (Figures 5E and 5H). These results indicate that the rapid permeabilization of *A. baumannii* membranes is followed by a marked drop in the reducing power of the bacterium. Judging from the similar decrease in replication rates (Figure 5E) and increase in numbers of dead cells (Figure 5H), this drop is likely irreversible.

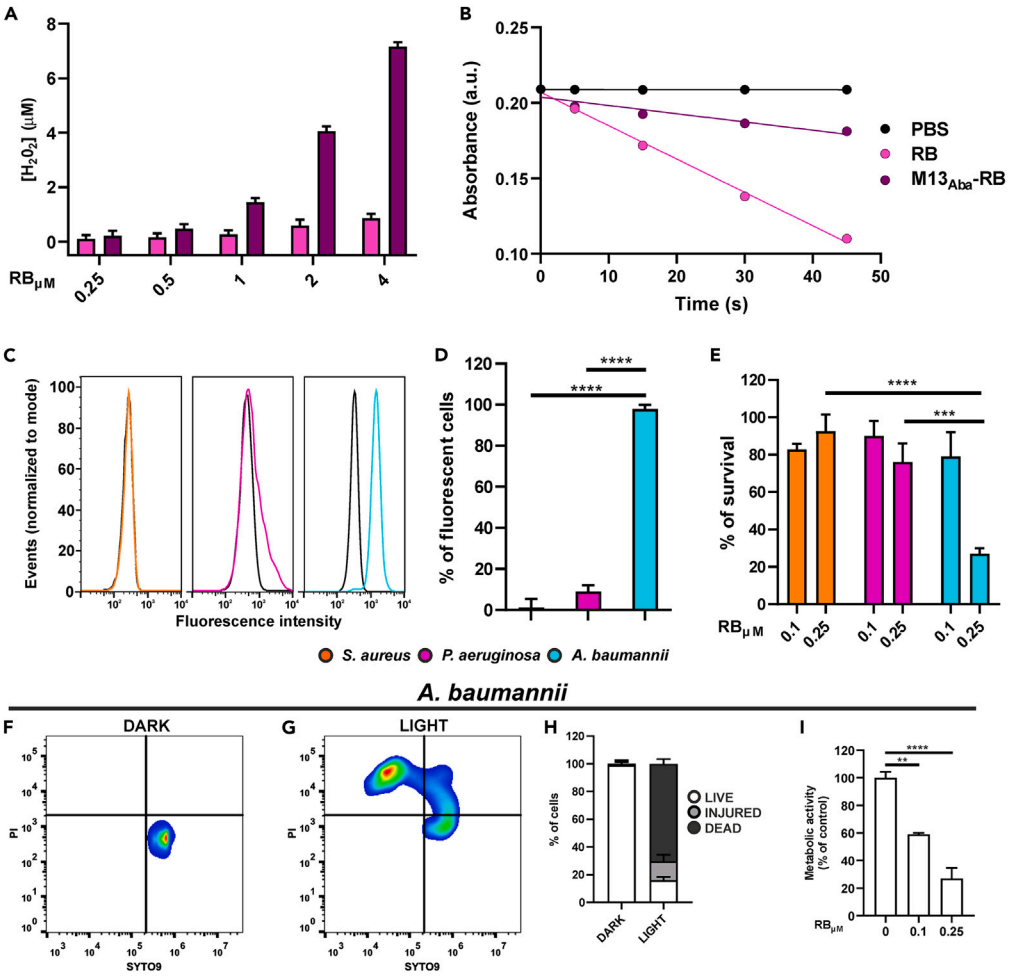

Figure 5. Photodynamic properties of M13Aba-RB

(A) Amplex Red assay for the generation of peroxides using different concentrations of RB (pink) and $M13_{Aba}$-RB (purple).

(B) Determination of $^1O_2$ generation following the decrease of ABMDMA absorbance over the irradiation time under white light irradiation for RB (pink line), $M13_{Aba}$-RB (purple line), and PBS (black line).

(C) Flow cytometry analysis of refactored and RB-conjugated $M13_{Aba}$-RB targeting to *S. aureus* (orange), *P. aeruginosa* (magenta), and *A. baumannii* (cyan). The fluorescence, detected in the PE channel, is related to RB.

(D–G) (D) Percentage of fluorescent cells at the flow cytometer. (E) Selective photodynamic killing of *S. aureus* (orange), *P. aeruginosa* (magenta), and *A. baumannii* (cyan) after 45 min of light irradiation following incubation with 0.1 and 0.25 μM (RB equivalents) of photoactive $M13_{Aba}$-RB. Live/dead assays were performed on *A. baumannii* cells preincubated with $M13_{Aba}$-RB and (F) kept in dark conditions or (G) irradiated.

(H) percentage of live, injured, and dead cells measured in the live/dead assay, 20 min post-irradiation.

(I) Metabolic activity of *A. baumannii* cells after phage-mediated aPDT. Data are represented as mean ± SD. ** = $p < 0.01$, *** = $p < 0.001$, **** = $p < 0.0001$.

Retargeting of the M13 platform against Gram-negative bacteria

We next investigated whether the tropism of the phage vector platform could be broadened to target not a single species such as *A. baumannii*, but Gram(−) bacteria in general. To this sake, a new phagemid was constructed (pPK_LPS), allowing for the multivalent display of a lipopolysaccharide (LPS)-binding peptide (KNYSSSISSIRAC) in fusion with the C-terminus of the pIII protein. LPS represents a major component of the outer membrane of Gram-negative bacteria and is a proven key virulence factor for *P. aeruginosa* and *A. baumannii* species.[46,47] The KNYSSSISSIRAC peptide exhibits two basic residues, but it is generally hydrophilic and was selected because it has a known high binding affinity to LPS.[48]

After co-transformation with the ΔpIII ΔF1ori helper phage plasmid, $M13_{Gram-}$ virions were produced and purified (Figure 6A). Immunoblotting with a pIII-C-term-specific antibody demonstrated the correct phage display of the LPS-binding peptide with the C-terminal domain of pIII (Figure 6B). Moreover, AFM analysis showed that the engineered $M13_{Gram-}$ virions are stable and uniform in their shortened size, packaging only the pPK_LPS phagemid (Figures 6D and 6E).

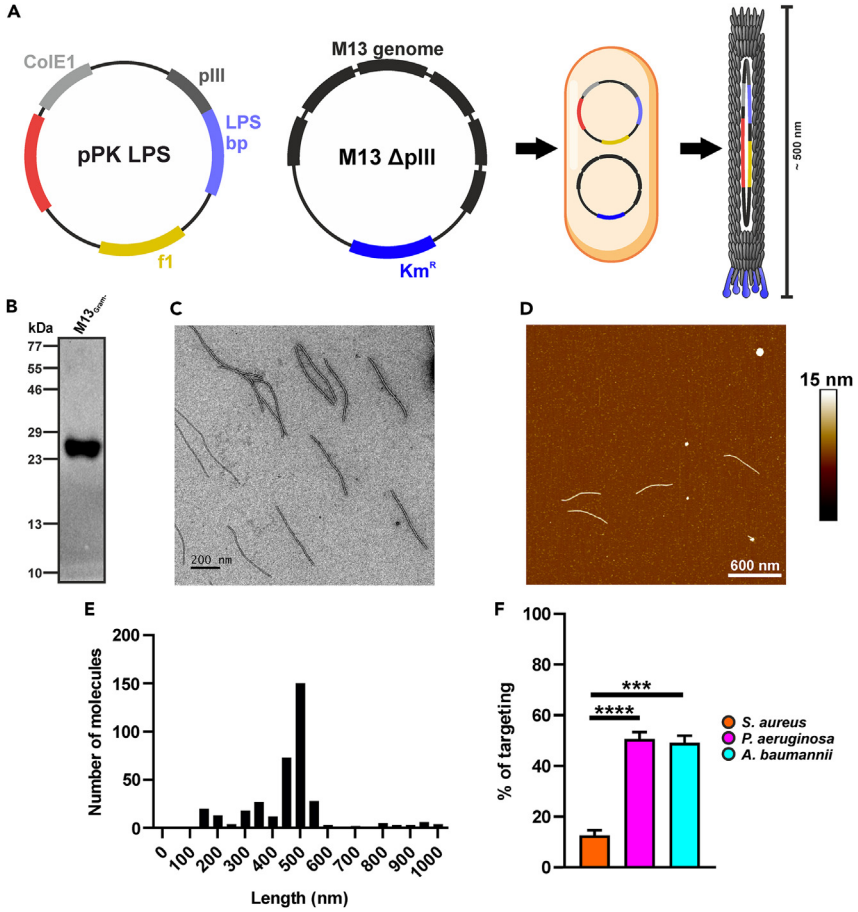

Figure 6. Characterization of the anti-Gram phage M13$_{Gram-}$

(A) Schematic representation of the M13 genetic engineering through co-transformation in *E. coli* of pPK_LPS phagemid and hyperphage genome.

(B–F) (B) Immunoblotting of the KNYSSSISSIRAC-pIII fusion (M13$_{Gram-}$) demonstrating incorporation in the purified virion. Visualization of purified M13$_{Gram-}$ phage through (C) TEM (scale bar = 200 nm) and (D) AFM (scale bar = 600 nm). (E) M13$_{Gram-}$ length distribution analyzed by AFM. (F) Selective tropism of engineered M13$_{Gram-}$ to Gram-negative bacteria was proved through targeting assays performed on *S. aureus* (orange), *P. aeruginosa* (magenta), and *A. baumannii* (cyan). Data are represented as mean ± SD. *** = $p < 0.001$, **** = $p < 0.0001$.

As for the M13$_{Aba}$ vector, the effective retargeting of M13$_{Gram-}$ virions was investigated by qPCR on the same panel of bacterial pathogens used before, including *P. aeruginosa* and *A. baumannii* as Gram-negatives, as well as *S. aureus* as Gram(+) control. M13$_{Gram-}$ proved to bind significantly better in targeting Gram(−) bacteria, with 50.6% ± 2.6% of the virions binding to *P. aeruginosa* and 49.1% ± 2.8% to *A. baumannii*, whereas significantly less phages (12.6% ± 2.0%) bound to *S. aureus*. These data indicate a broadened specificity of the retargeted M13$_{Gram-}$ phage for Gram(−) bacteria expressing LPS on their surface (Figure 6F).

Potent phage-mediated PDT against antibiotic-resistant Gram(−) bacteria

The retargeted M13$_{Gram-}$ phages were then conjugated with RB, and purified from unreacted sensitizer molecules, as previously described. Again, the generation of peroxide of the bioconjugate increased 8-fold, whereas the production of the singlet oxygen decreased 4-fold (φ_Δ decrease from 0.76 to 0.20), compared with free RB.

These results indicate that the LPS-binding phages retain similar ROS generating rates to their M13 and M13$_{Aba}$ counterparts (Figures 7A and 7B), testifying reproducible results of the vector platform after retargeting.

To demonstrate that the tropism toward Gram(−) bacteria was not altered after conjugation with RB, flow cytometry experiments with M13$_{Gram-}$-RB were carried out (Figures 7C and 7D). Clearly, the phage vector bound to both *A. baumannii* and *P. aeruginosa*, whereas no fluorescence shift was observed for *S. aureus*. In particular, the totality (100%) of *A. baumannii* cells was labeled and detected after incubation with M13$_{Gram-}$-RB; slightly lower rates were recorded for *P. aeruginosa* (70%), whereas only 7% of *S. aureus* cells were targeted by the phage, suggesting an intact specificity of M13$_{Gram-}$ for Gram(−) bacteria, even after chemical conjugation.

Photodynamic antimicrobial assays were eventually set up to investigate the specificity of M13$_{Gram-}$-RB in killing preferentially Gram(−) bacteria. Bacteria were treated with different concentrations of the phage bioconjugate and irradiated with the same settings

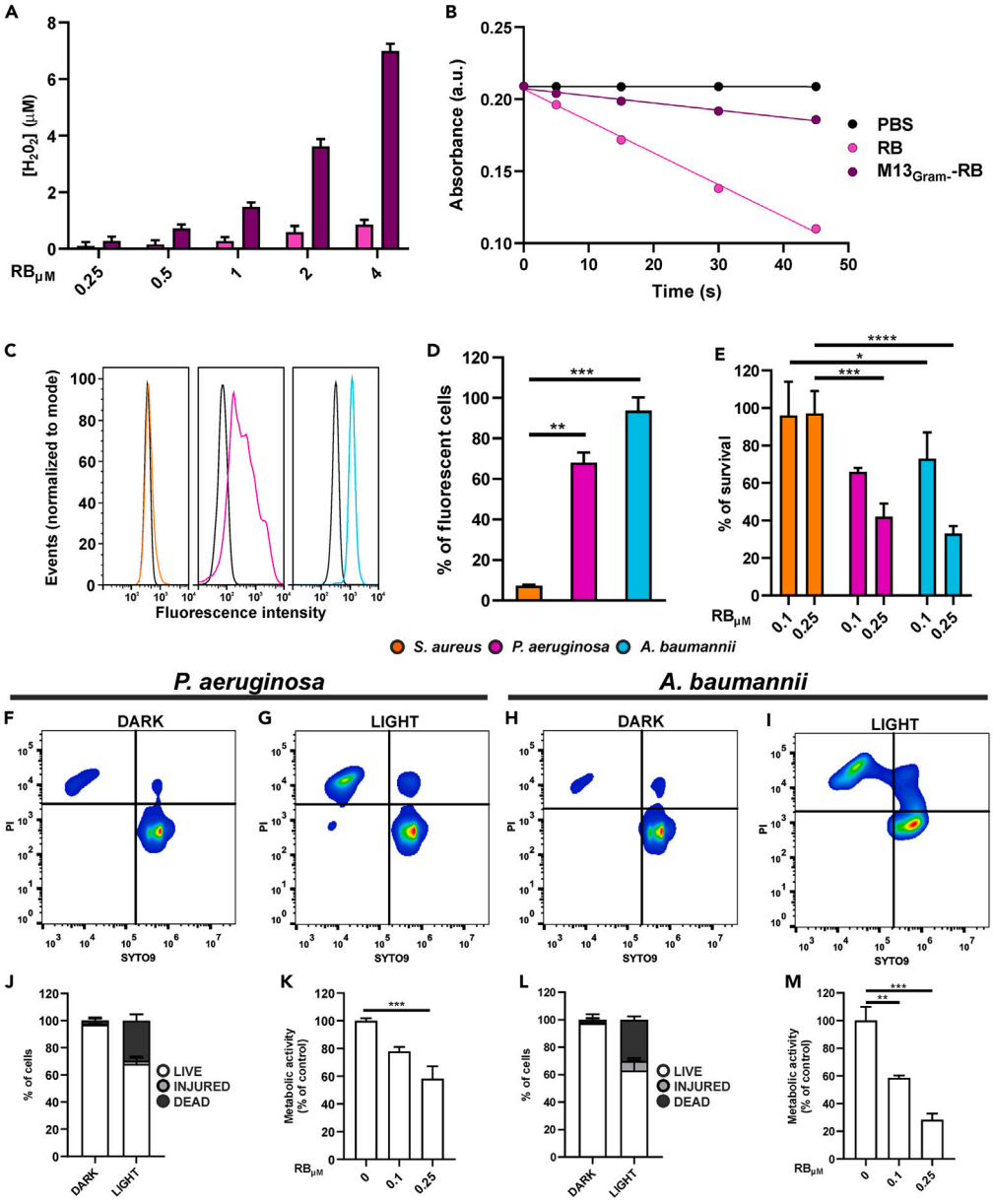

Figure 7. Photodynamic properties of the $M13_{Gram-}$ phage vector

(A) Amplex Red assay for the generation of peroxides using different concentrations of RB (pink) and $M13_{Gram-}$-RB (purple).

(B) Determination of $^1O_2$ generation following the decrease of ABMDMA absorbance over the irradiation time under white light irradiation for RB (pink line), $M13_{Gram-}$-RB (purple line), and PBS (black line).

(C) Flow cytometry analysis of retargeted and RB-conjugated $M13_{Gram-}$ phages directed to the lipopolysaccharides of Gram-negative bacteria: dark lines correspond to the control cells treated with PBS, whereas colored ones highlight binding of the engineered $M13_{Gram-}$-RB to *S. aureus* (orange), *P. aeruginosa* (magenta), and *A. baumannii* (cyan).

(D) Percentage of bacterial fluorescent cells measured by flow cytometry analysis.

(E–I) (E) Percentage of bacteria survived to light irradiation after preincubation with $M13_{Gram-}$-RB phages. The activity of phages was tested at two concentrations, 0.1 and 0.25 μM, of equivalent RB. Live/dead assay was performed on *P. aeruginosa* and *A. baumannii* preincubated with $M13_{Gram-}$-RB and (F–H) kept in dark or (G–I) irradiated.

(J–M) Percentage of live, injured, and dead cells measured in live/dead assay 20 min after irradiation. Metabolic activity of (K) *P. aeruginosa* and (M) *A. baumannii* after phage-mediated aPDT. Data are represented as mean ± SD. * = $p < 0.05$, ** = $p < 0.01$, *** = $p < 0.001$, **** = $p < 0.0001$.

used for $M13_{Aba}$. Again, $M13_{Gram-}$-RB vector showed no antimicrobial effects when bacteria were kept in the dark, whereas irradiation provoked a significant reduction in survival rates only for *A. baumannii* and *P. aeruginosa* (Figure 7E). In both cases, a dose-dependent effect could be observed at pM phage concentrations, with higher vector concentrations and RB equivalents correlating with increased light-dependent antimicrobial effects. On the contrary, neither of the two vector concentrations tested showed effective in antimicrobial photodynamic therapy (aPDT) on *S. aureus*, suggesting that $M13_{Gram-}$-RB is harmless against Gram(+) cells. As for $M13_{Aba}$-RB (Figure 5), additional live/dead and metabolic assays were carried out to validate the photodynamic proprieties of $M13_{Gram-}$-RB on *P. aeruginosa* and *A. baumannii*. Both species showed a consistent shift in the live-dead staining after incubation with $M13_{Gram-}$-RB and irradiation (Figures 7F and 7G for *P. aeruginosa*; Figures 7H and 7I for *A. baumannii*), albeit at lower permeabilization rates (30%–40% PI positive cells) (respectively, Figures 7J and 7L), suggesting weaker photodynamic performances of $M13_{Gram-}$-RB with respect to $M13_{Aba}$-RB (>70% PI positive cells; Figure 5H). The metabolic assays confirmed this trend both for *P. aeruginosa* (Figure 7K) as well as for *A. baumannii* (Figure 7M) with a more pronounced decrease of the metabolic activity for the latter. These results indicate that the phage- and light-dependent permeabilization of membranes is followed by a pursuant drop in the metabolic activity of bacteria targeted by the vector.

DISCUSSION

Our results demonstrate that engineered M13 phages can serve as potent vectors for antimicrobial PDT and that their tropism can be conveniently tweaked to target specifically diverse Gram(−) bacterial pathogens. Light-activated killing of microorganisms represents a promising alternative to treat antibiotic-resistant infections.

Phages, in their own right, represent eclectic antibacterial solutions. Classic phage therapy with natural phages has provided a useful tool before the advent of antibiotics and is receiving renewed attention for treating antibiotic-resistant pathogens. However, the intimate co-evolution of phages with specific bacterial strains results in intrinsic therapeutic limitations. Natural phages generally sport a very restricted host range, variable antibacterial (lytic) efficacy, and frequent emergence of host resistance against phage infection and propagation.[8,49] The lack of full biological characterization of many natural phage preparations may present further risks due to the possible transduction of virulence genes.[50] In addition, the complex and varying pharmacokinetics and pharmacodynamics of different phages constitute a major challenge for clinical translation.[8,51–53]

As such, there is a growing consensus over the idea that designer strategies, including synthetic biology and nanotechnology approaches on well-studied model phages, could contribute to overcome some constraints of classic phage therapy, for example, providing engineered phages with new (modular) functions, tailored host ranges, improved safety profiles, and a more reproducible pharmacological behavior.[54–58]

M13 represents an excellent platform for aPDT, with significant advantages over other active targeting schemes (recently reviewed in[24]). Taking advantage of the long-standing and straightforward molecular toolkit available for this simple phage,[59] targeting moieties such as peptides and antibodies can be genetically displayed on g3p at one tip of the recombinant virion, much alike the bits of a modular screwdriver. This leaves the large number of g8p capsomers available for functionalization with hundreds of sensitizers. The exposed domain of g8p (pVIII) harbors accessible and reactive amino acids such as the lysine residues, the aromatic groups of tyrosine, and carboxylic acid groups of acidic residues, which can be combined with functional derivatives in simple processes including EDC/NHS activation, maleimide-thiol coupling, diazonium reagents, and click chemistry.[60,61]

The pentavalent display of the targeting moiety on g3p together with the high sensitizer payload allows respectively to (1) exploit possible cooperative binding effects of the targeting moieties displayed on g3p and (2) increase ROS generation only in close proximity of the pathogen, reaching lethal Gram(−) photosensitization at sub-micromolar concentrations of the vector, without losing specificity (Figures 5 and 7). This result indicates that the ROS produced extracellularly by the M13 platform in aPDT can be very effective without need of photosensitizer internalization. The dispensability of sensitizer internalization was similarly determined for a study on photobactericidal activity of porphyrin–cellulose nanocrystals (CNC-Por) against *A. baumannii*.[62] However, the use of a phage scaffold allowed to attain similar killing effects with >100-fold reduction in sensitizer concentration as compared with CNC-Por. Also, for the other Gram(−) bacteria tested in this study, lethal photosensitization occurred at sub-micromolar RB concentrations when the sensitizer was conjugated to the M13 vector (Figures 3 and 7, respectively for *E. coli* and *P. aeruginosa*). By contrast, significantly higher concentrations of RB (10–100 μM) were needed to observe photoinhibition effects when the bare sensitizer was administered to planktonic Gram(−) bacteria or biofilms ([63,64], and data not shown). These results are particularly interesting when we also consider that Gram(−) bacteria, due to different cell wall structure, are more resistant to aPDT than Gram(+) bacteria.[65] The effectiveness at lower sensitizer concentrations may be important to reduce side effects but also to overcome the limitations of suboptimal irradiation intensities deriving from the poor penetration of light (see below).

These results add to the evidence that important improvements can be obtained in aPDT when routing the sensitizers with bacteriophage-sensitizer nanoconjugates, likely because of the higher sensitizer payload of the phage scaffolds. A pioneering study in which natural phages were conjugated with chlorine e6 demonstrated for the first time that a phage can be used to deliver photosensitizers to a target organism/cell, resulting in enhanced photosensitization and killing of *S. aureus*.[34] This approach relied on natural phages, limiting the host range to specific species or strains. More recently, a difunctional bacteriophage, displaying a scFv for specific binding to *Candida albicans* and armed with pheophorbide (PPA), a chlorophyll-based photosensitizer, was used for fungal photodynamic inactivation. The PPa-JM-phage nanobioconjugate was shown to trigger light-dependent killing of *C. albicans* through a caspase-dependent (apoptotic) pathway.[35,66]

To date, the best evidence for the potential of designer phage nanobioconjugates in photodynamic antimicrobial treatments is represented by M13 phages conjugated to gold nanorods or nanoparticles.[35,66] The latter can be excited by light in the near-infrared (NIR) window, translating the light energy into heat and creating extremely high local temperatures useful for photothermal therapy (PTT).[67,68] In one study, M13 phanorods were retargeted to bind selectively *P. aeruginosa* through pIII-display of the orthologous receptor-binding domain of the *P. aeruginosa*-specific filamentous PF1 phage. Following their functionalization with gold nanorods, the conjugates were shown to eradicate *P. aeruginosa* biofilms after NIR irradiation, provoking only minor cytotoxicity to bystander mammalian cells, co-cultured with the bacteria. Notably, the irradiation also destroyed the phage vector, reducing potential risks of phage replication and horizontal gene transfer associated with classic phage therapy.[35] More recently, the derivatization of phanorods with Zn^{2+}-releasing peptides allowed to counter antibiotic-resistant *P. aeruginosa* wound infections *in vivo*, showing no detectable toxicity or systemic effects in mice following wound irradiation.[69] As for phanorods, the proficient targeting and negligible side effects of the M13-RB bioconjugates need to be confirmed in an appropriate animal infection model, to validate the applicability for *in vivo* bacterial control.

Our results further add to these evidences, highlighting the advantage of phage-based targeting in photodynamic antimicrobial therapies. This potential is boosted by the possibility to rationally modify (change, narrow, or broaden) their tropism: we show that the targeting moieties, achieving specificity against different bacterial hosts, are not limited to the repertoire of characterized receptor-binding domains of natural phages, but also include simple peptides and stable monomeric sdAb (or scFv) scaffolds, expanding the choice to a wide portfolio of peptides, immunoglobulin (Ig) folds, and other non-Ig domains able to bind to bacteria. In particular, the broadening of the target spectrum, achieved by genetic display of an LPS-binding peptide (Figure 6), may be important if several Gram(−) pathogens need to be targeted at once or in cases where more specific targeting moieties are not available. Similarly, the receptor-binding domains of several phages with broad host range[70] could serve for this purpose.

Among the advantages of antimicrobial photodynamic therapy is that the killing mechanism relies on physical damage of the biomolecules, thereby acting also on metabolically inactive or even antibiotic-resistant cells.[22] ROS produced by aPDT also affect and impair lipopolysaccharide,[71] leading to an immediate onset of membrane damage[25] (as also evident from the live/dead assays in Figures 5G, 7G, and 7I). As such, aPDT seems exempt from the selection of resistant strains, even after repeated cycles of treatment.[72] One study reported that initial exposure to low doses of antibacterial blue light (aBL, 405 nm) eventually increased the tolerance of methicillin-susceptible *S. aureus* to higher doses of violet light, possibly because of upregulation of bacterial stress responses.[73] However, a second set of experiments showed that repeated sub-lethal aBL irradiations did not trigger photodynamic tolerance in *S. aureus*.[74] Moreover, the dual daily administration of Indocyanine green (ICG), triggered with near-infrared 810 nm light for aPDT, combined with 405 nm aBL resulted in a sustained antibacterial effect on *S. aureus*.[75] These results speak in favor of limited risks for developing resistance against aPDT.

On the other hand, aPDT may be affected by low specificity for target cells, whereas the photosensitizers could have low bioavailability *per se* in the absence of carriers (e.g., poor solubility, dispersion). Our results indicate that engineered M13 virions are not damaged by extensive conjugation with the photosensitizers. This was not predictable as the conjugated molecules may alter the solubility, monodispersion, or charge of the phage, which in turn could impair target recognition and specificity. Moreover, as the phage acts as a suicide vector, with the only scope to vehiculate sensitizers to the target cells, the downstream evolution of resistance mechanisms against phage replication and cell lysis, which frequently plagues classic phage therapy, becomes irrelevant.

For non-invasive applications, the penetration of light into tissue is highly dependent on the wavelength. Therefore, aPDT is currently best suited for topic applications, directly accessible to irradiation sources that can produce light intensities sufficient to activate the photosensitizers. Building on the improvement of irradiation and optical fiber systems, also employed in anti-cancer PDT approaches,[76,77] aPDT could in principle be suitable to treat deeper infections and abscesses. For example, the use of sensitizers activable with laser light in the near-infrared (NIR) window allows to extend PDT approaches to subcutaneous settings, up to 3 cm deep in the tissues.[78] Ultrasound has also been used to activate certain photosensitizers, including Rose Bengal.[79] Antimicrobial sonodynamic therapy (aSDT) with RB-conjugated phages could therefore present several advantages to achieve lethal sensitization even deeper in the body than visible light or NIR.[80,81]

In general, photodynamic therapy seems to be a viable alternative for treating infections caused by ESKAPEE bacteria, especially for topical use. We anticipate that engineered model phages and self-assembling (virus-like) nanoparticles will provide excellent platforms for delivering sensitizers as well as antimicrobial drugs for targeted treatments. Furthermore, synergistic effects can be obtained by aPDT when combined with antibiotics, antimicrobial peptides, nanoparticles, or efflux pump inhibitors. This study shows that M13 can be engineered from an evolving biological entity with a limited host-range into a controlled, nanoparticle-like reagent with a high sensitizer payload.

In principle this nanobot may be retargeted to any cell if a targeting peptide or moiety can be fused to the g3p protein. In this scheme the possible mechanisms to develop resistance are likely to be constrained to mutations in the chosen receptor or in the acquisition of exceptionally robust ROS detoxification mechanisms.

Limitations of the study

Our study presents a novel modular phage vector platform for the application of antimicrobial photodynamic therapy against Gram-negative bacterial pathogens. However, there are a number of limitations to our study to be pointed out. First, a potential limitation of targeting M13 against *A. baumannii* by expressing the C20 nanobody fused with the pIII protein is the variability of the BAP protein among all *A. baumannii* strains. Although the gene is conserved in nearly all strains of *A. baumannii*, variations in the coding sequence, such as insertions, deletions, or mutations, could alter the binding epitope and hinder efficient phage targeting.[82] To overcome this challenge, $M13_{Gram-}$ can be employed, as it has the ability to target broadly Gram(−) bacteria, including *A. baumannii*. Alternatively, the modular nature of our platform can be

exploited by displaying other targeting moieties specific for *A. baumannii*, in fusion with the pIII protein of M13. As a proof of concept in this study, both wild-type M13 phage and engineered phages were conjugated with the photosensitizer Rose Bengal. However, this does not exclude the possibility that other photosensitizers may exhibit improved efficiency in generating ROS and subsequent increased antimicrobial photodynamic therapy (aPDT) effects on pathogens. Considering the wide range of available sensitizers to choose from, the effective potential on phage-mediated aPDT may be further validated and expanded.[83–85] The selection of a specific sensitizer can also be based on therapeutic needs. For instance, the use of sensitizers excitable with infrared lasers allows for deeper tissue penetration of light, enabling the treatment of subcutaneous infections.[85] Lastly, our investigations were limited to *in vitro* experiments, in order to provide a first proof-of-principle of the technology and did not involve *in vivo* animal models. To fully comprehend the potential of engineered phages rigged for aPDT in targeting bacterial infections, it will be important to explore the challenges associated with animal treatments. This would involve investigating different modes of phage administration, such as intraperitoneal, intravenous, or local injection, to determine the optimal approach for targeting the infections. In addition, the efficacy of phage administration may vary depending on the bacterial species and the region of infection. Therefore, further research is needed to evaluate the applicability of our platform in diverse infection models.

STAR★METHODS

Detailed methods are provided in the online version of this paper and include the following:

- KEY RESOURCES TABLE
- RESOURCE AVAILABILITY
  - Lead contact
  - Materials availability
  - Data and code availability
- EXPERIMENTAL MODEL AND STUDY PARTICIPANT DETAILS
- METHOD DETAILS
  - Bacterial cultures
  - Phagemid cloning and phage preparation
  - Transmission electron microscopy (TEM) analysis
  - AFM analysis of engineered phages
  - Immunoblotting
  - Validation of phage retargeting by qPCR
  - Bioconjugation and purification of M13-RB, $M13_{Aba}$ and $M13_{Gram-}$ phages
  - Singlet oxygen assay
  - Peroxides assay
  - Validation of phage retargeting by flow cytometry
  - Antimicrobial PDT assays
- QUANTIFICATION AND STATISTICAL ANALYSIS

ACKNOWLEDGMENTS

This research was supported by a CARISBO grant (Ricerca Medica e Alta Tecnologia 2021), AIRC under the MFAG 2019 ID. 22894 project (P.I.: M.C.), and EU funding within the NextGeneration EU-MUR PNRR Extended Partnership initiative on Emerging Infectious Diseases (Project no. PE00000007, INF-ACT) and from the Horizon Pathfinder Open programme under Grant Agreement N10104678ECLipse. A.D. was supported by a Proof-of-Concept grant by the Italian Ministry of Economic Development and the University of Bologna. The support from the Italian MUR (PRIN2022, PhageTarget project 2022K452FJ) is gratefully acknowledged.

AUTHOR CONTRIBUTIONS

Investigation, Data Curation, Formal Analysis: A.P., R.S., F.S., E.S., L.U., L.B., A.C., A.M., S.K.Z., G.Z., Z.P., M.D.G., and P.E.C. Conceptualization, Formal Analysis, Funding Acquisition, Methodology, Supervision: L.P. P.P.P., P.E.C, M.C., and A.D. Writing: all authors.

DECLARATION OF INTERESTS

There are no conflicts to declare.

Received: May 17, 2023
Revised: August 4, 2023
Accepted: September 21, 2023
Published: September 27, 2023

REFERENCES

1. Strathdee, S.A., Hatfull, G.F., Mutalik, V.K., and Schooley, R.T. (2023). Phage therapy: From biological mechanisms to future directions. Cell *186*, 17–31. https://doi.org/10.1016/J.CELL.2022.11.017.
2. Uyttebroek, S., Chen, B., Onsea, J., Ruythooren, F., Debaveye, Y., Devolder, D., Spriet, I., Depypere, M., Wagemans, J., Lavigne, R., et al. (2022). Safety and efficacy of phage therapy in difficult-to-treat infections: a systematic review. Lancet Infect. Dis. *22*, e208–e220. https://doi.org/10.1016/S1473-3099(21)00612-5.
3. Pirnay, J.P., and Kutter, E. (2021). Bacteriophages: it's a medicine, Jim, but not as we know it. Lancet Infect. Dis. *21*, 309–311. https://doi.org/10.1016/S1473-3099(20)30464-3.
4. Schooley, R.T., Biswas, B., Gill, J.J., Hernandez-Morales, A., Lancaster, J., Lessor, L., Barr, J.J., Reed, S.L., Rohwer, F., Benler, S., et al. (2017). Development and use of personalized bacteriophage-based therapeutic cocktails to treat a patient with a disseminated resistant Acinetobacter baumannii infection. Antimicrob. Agents Chemother. *61*, e00954-17. https://doi.org/10.1128/AAC.00954-17.
5. Berryhill, B.A., Huseby, D.L., McCall, I.C., Hughes, D., and Levin, B.R. (2021). Evaluating the potential efficacy and limitations of a phage for joint antibiotic and phage therapy of Staphylococcus aureus infections. Proc. Natl. Acad. Sci. USA *118*, e2008007118. https://doi.org/10.1073/PNAS.2008007118.
6. Van Nieuwenhuyse, B., Van der Linden, D., Chatzis, O., Lood, C., Wagemans, J., Lavigne, R., Schroven, K., Paeshuyse, J., de Magnée, C., Sokal, E., et al. (2022). Bacteriophage-antibiotic combination therapy against extensively drug-resistant Pseudomonas aeruginosa infection to allow liver transplantation in a toddler. Nat. Commun. *13*, 5725–5812. https://doi.org/10.1038/s41467-022-33294-w.
7. Gordillo Altamirano, F.L., Kostoulias, X., Subedi, D., Korneev, D., Peleg, A.Y., and Barr, J.J. (2022). Phage-antibiotic combination is a superior treatment against Acinetobacter baumannii in a preclinical study. EBioMedicine *80*, 104045. https://doi.org/10.1016/J.EBIOM.2022.104045.
8. Dąbrowska, K., and Abedon, S.T. (2019). Pharmacologically aware phage therapy: pharmacodynamic and pharmacokinetic obstacles to phage antibacterial action in animal and human bodies. Microbiol. Mol. Biol. Rev. *83*, e00012–e00019. https://doi.org/10.1128/MMBR.00012-19.
9. Wang, R., Li, H.D., Cao, Y., Wang, Z.Y., Yang, T., and Wang, J.H. (2023). M13 phage: a versatile building block for a highly specific analysis platform. Anal. Bioanal. Chem. *415*, 3927–3944. https://doi.org/10.1007/S00216-023-04606-W.
10. Henry, K.A., Arbabi-Ghahroudi, M., and Scott, J.K. (2015). Beyond phage display: non-traditional applications of the filamentous bacteriophage as a vaccine carrier, therapeutic biologic, and bioconjugation scaffold. Front. Microbiol. *6*, 755. https://doi.org/10.3389/fmicb.2015.00755.
11. Sperandio, F.F., Huang, Y.-Y., and Hamblin, M.R. (2013). Antimicrobial photodynamic therapy to kill Gram-negative bacteria. Recent Pat. Anti-Infect. Drug Discov. *8*, 108–120. https://doi.org/10.2174/1574891X113089990012.
12. Shi, H., and Sadler, P.J. (2020). How promising is phototherapy for cancer? Br. J. Cancer *123*, 871–873. https://doi.org/10.1038/s41416-020-0926-3.
13. Dolmans, D.E.J.G.J., Fukumura, D., and Jain, R.K. (2003). Photodynamic therapy for cancer. Nat. Rev. Cancer *3*, 380–387. https://doi.org/10.1038/NRC1071.
14. Yin, R., Agrawal, T., Khan, U., Gupta, G.K., Rai, V., Huang, Y.Y., and Hamblin, M.R. (2015). Antimicrobial photodynamic inactivation in nanomedicine: small light strides against bad bugs. Nanomedicine *10*, 2379–2404. https://doi.org/10.2217/NNM.15.67.
15. Li, X., Lovell, J.F., Yoon, J., and Chen, X. (2020). Clinical development and potential of photothermal and photodynamic therapies for cancer. Nat. Rev. Clin. Oncol. *17*, 657–674. https://doi.org/10.1038/s41571-020-0410-2.
16. Cieplik, F., Deng, D., Crielaard, W., Buchalla, W., Hellwig, E., Al-Ahmad, A., and Maisch, T. (2018). Antimicrobial photodynamic therapy - what we know and what we don't. Crit. Rev. Microbiol. *44*, 571–589. https://doi.org/10.1080/1040841X.2018.1467876.
17. Hu, X., Huang, Y.Y., Wang, Y., Wang, X., and Hamblin, M.R. (2018). Antimicrobial photodynamic therapy to control clinically relevant biofilm infections. Front. Microbiol. *9*, 1299. https://doi.org/10.3389/FMICB.2018.01299.
18. Tomb, R.M., White, T.A., Coia, J.E., Anderson, J.G., MacGregor, S.J., and Maclean, M. (2018). Review of the comparative susceptibility of microbial species to photoinactivation using 380-480 nm violet-blue Light. Photochem. Photobiol. *94*, 445–458. https://doi.org/10.1111/PHP.12883.
19. Wozniak, A., and Grinholc, M. (2018). Combined antimicrobial activity of photodynamic inactivation and antimicrobials-state of the art. Front. Microbiol. *9*, 930. https://doi.org/10.3389/FMICB.2018.00930.
20. Tanaka, M., Mroz, P., Dai, T., Huang, L., Morimoto, Y., Kinoshita, M., Yoshihara, Y., Nemoto, K., Shinomiya, N., Seki, S., and Hamblin, M.R. (2012). Photodynamic therapy can induce a protective innate immune response against murine bacterial arthritis via neutrophil accumulation. PLoS One *7*, e39823. https://doi.org/10.1371/JOURNAL.PONE.0039823.
21. Barra, F., Roscetto, E., Soriano, A.A., Vollaro, A., Postiglione, I., Pierantoni, G.M., Palumbo, G., and Catania, M.R. (2015). Photodynamic and antibiotic therapy in combination to fight biofilms and resistant surface bacterial infections. Int. J. Mol. Sci. *16*, 20417–20430. https://doi.org/10.3390/IJMS160920417.
22. Garcez, A.S., Nuñez, S.C., Hamblim, M.R., Suzuki, H., and Ribeiro, M.S. (2010). Photodynamic therapy associated with conventional endodontic treatment in patients with antibiotic-resistant microflora: a preliminary report. J. Endod. *36*, 1463–1466. https://doi.org/10.1016/J.JOEN.2010.06.001.
23. Takasaki, A.A., Aoki, A., Mizutani, K., Schwarz, F., Sculean, A., Wang, C.Y., Koshy, G., Romanos, G., Ishikawa, I., and Izumi, Y. (2009). Application of antimicrobial photodynamic therapy in periodontal and peri-implant diseases. Periodontology *51*, 109–140. https://doi.org/10.1111/J.1600-0757.2009.00302.X.
24. Thomas-Moore, B.A., del Valle, C.A., Field, R.A., and Marín, M.J. (2022). Recent advances in nanoparticle-based targeting tactics for antibacterial photodynamic therapy. Photochem. Photobiol. Sci. *21*, 1111–1131. https://doi.org/10.1007/S43630-022-00194-3.
25. Cantelli, A., Piro, F., Pecchini, P., Di Giosia, M., Danielli, A., and Calvaresi, M. (2020). Concanavalin A-Rose Bengal bioconjugate for targeted Gram-negative antimicrobial photodynamic therapy. J. Photochem. Photobiol., B *206*, 111852. https://doi.org/10.1016/J.JPHOTOBIOL.2020.111852.
26. Cao, B., Xu, H., Yang, M., and Mao, C. (2018). Virus-based cancer therapeutics for targeted photodynamic therapy. Methods Mol. Biol. *1776*, 643–652. https://doi.org/10.1007/978-1-4939-7808-3_41.
27. Cohen, B.A., and Bergkvist, M. (2013). Targeted in vitro photodynamic therapy via aptamer-labeled, porphyrin-loaded virus capsids. J. Photochem. Photobiol., B *121*, 67–74. https://doi.org/10.1016/J.JPHOTOBIOL.2013.02.013.
28. Ariga, K., Leong, D.T., and Mori, T. (2018). Nanoarchitectonics for hybrid and related materials for bio-oriented applications. Adv. Funct. Mater. *28*, 1702905. https://doi.org/10.1002/ADFM.201702905.
29. Kalarical Janardhanan, S., Narayan, S., Abbineni, G., Hayhurst, A., and Mao, C. (2010). Architectonics of phage-liposome nanowebs as optimized photosensitizer vehicles for photodynamic cancer therapy. Mol. Cancer Therapeut. *9*, 2524–2535. https://doi.org/10.1158/1535-7163.MCT-10-0253.
30. Deken, M.M., Kijanka, M.M., Beltrán Hernández, I., Slooter, M.D., de Bruijn, H.S., van Diest, P.J., van Bergen en Henegouwen, P.M.P., Lowik, C.W.G.M., Robinson, D.J., Vahrmeijer, A.L., and Oliveira, S. (2020). Nanobody-targeted photodynamic therapy induces significant tumor regression of trastuzumab-resistant HER2-positive breast cancer, after a single treatment session. J. Contr. Release *323*, 269–281. https://doi.org/10.1016/J.JCONREL.2020.04.030.
31. Ulfo, L., Costantini, P.E., Di Giosia, M., Danielli, A., and Calvaresi, M. (2022). EGFR-targeted photodynamic therapy. Pharmaceutics *14*, 241. https://doi.org/10.3390/PHARMACEUTICS14020241.
32. Jia, H.R., Zhu, Y.X., Chen, Z., and Wu, F.G. (2017). Cholesterol-assisted bacterial cell surface engineering for photodynamic inactivation of Gram-positive and Gram-negative Bacteria. ACS Appl. Mater. Interfaces *9*, 15943–15951. https://doi.org/10.1021/ACSAMI.7B02562.
33. Jia, H.R., Zhu, Y.X., Liu, Y., Guo, Y., Sayed, S.M., Zhu, X.Y., Cheng, X., and Wu, F.G. (2022). Direct chemical editing of Gram-positive bacterial cell walls via an enzyme-catalyzed oxidative coupling reaction. Explorations *2*, 20220010. https://doi.org/10.1002/EXP.20220010.
34. Embleton, M.L., Nair, S.P., Heywood, W., Menon, D.C., Cookson, B.D., and Wilson, M. (2005). Development of a novel targeting system for lethal photosensitization of antibiotic-resistant strains of Staphylococcus aureus. Antimicrob. Agents Chemother. *49*, 3690–3696. https://doi.org/10.1128/AAC.49.9.3690-3696.2005.

35. Peng, H., Borg, R.E., Dow, L.P., Pruitt, B.L., and Chen, I.A. (2020). Controlled phage therapy by photothermal ablation of specific bacterial species using gold nanorods targeted by chimeric phages. Proc. Natl. Acad. Sci. USA *117*, 1951–1961. https://doi.org/10.1073/pnas.1913234117.
36. Lee, J.-W., Song, J., Hwang, M.P., and Lee, K.H. (2013). Nanoscale bacteriophage biosensors beyond phage display. Int. J. Nanomed. *8*, 3917–3925. https://doi.org/10.2147/IJN.S51894.
37. Gandra, N., Abbineni, G., Qu, X., Huai, Y., Wang, L., and Mao, C. (2013). Bacteriophage bionanowire as a carrier for both cancer-targeting peptides and photosensitizers and its use in selective cancer cell killing by photodynamic therapy. Small *9*, 215–221. https://doi.org/10.1002/SMLL.201202090.
38. Ulfo, L., Cantelli, A., Petrosino, A., Costantini, P.E., Nigro, M., Starinieri, F., Turrini, E., Zadran, S.K., Zuccheri, G., Saporetti, R., et al. (2022). Orthogonal nanoarchitectonics of M13 phage for receptor targeted anticancer photodynamic therapy. Nanoscale *14*, 632–641. https://doi.org/10.1039/d1nr06053h.
39. Bortot, B., Apollonio, M., Baj, G., Andolfi, L., Zupin, L., Crovella, S., di Giosia, M., Cantelli, A., Saporetti, R., Ulfo, L., et al. (2022). Advanced photodynamic therapy with an engineered M13 phage targeting EGFR: Mitochondrial localization and autophagy induction in ovarian cancer cell lines. Free Radic. Biol. Med. *179*, 242–251. https://doi.org/10.1016/J.FREERADBIOMED.2021.11.019.
40. Demartis, S., Obinu, A., Gavini, E., Giunchedi, P., and Rassu, G. (2021). Nanotechnology-based rose Bengal: a broad-spectrum biomedical tool. Dyes Pigments *188*, 109236. https://doi.org/10.1016/J.DYEPIG.2021.109236.
41. Moczek, Ł., and Nowakowska, M. (2007). Novel water-soluble photosensitizers from chitosan. Biomacromolecules *8*, 433–438. https://doi.org/10.1021/bm060454+.
42. Russel, M., Whirlow, H., Sun, T.P., and Webster, R.E. (1988). Low-frequency infection of F- bacteria by transducing particles of filamentous bacteriophages. J. Bacteriol. *170*, 5312–5316. https://doi.org/10.1128/JB.170.11.5312-5316.1988.
43. Payandeh, Z., Rasooli, I., Mousavi Gargari, S.L., Rajabi Bazl, M., and Ebrahimizadeh, W. (2014). Immunoreaction of a recombinant nanobody from camelid single domain antibody fragment with Acinetobacter baumannii. Trans. R. Soc. Trop. Med. Hyg. *108*, 92–98. https://doi.org/10.1093/TRSTMH/TRT114.
44. Di Giosia, M., Bomans, P.H.H., Bottoni, A., Cantelli, A., Falini, G., Franchi, P., Guarracino, G., Friedrich, H., Lucarini, M., Paolucci, F., et al. (2018). Proteins as supramolecular hosts for C60: a true solution of C60 in water. Nanoscale *10*, 9908–9916. https://doi.org/10.1039/C8NR02220H.
45. Cantelli, A., Malferrari, M., Soldà, A., Simonetti, G., Forni, S., Toscanella, E., Mattioli, E.J., Zerbetto, F., Zanelli, A., Di Giosia, M., et al. (2021). Human serum albumin-oligothiophene bioconjugate: a phototheranostic platform for localized killing of cancer cells by precise light activation. JACS Au *1*, 925–935. https://doi.org/10.1021/JACSAU.1C00061.
46. Pier, G.B. (2007). Pseudomonas aeruginosa lipopolysaccharide: A major virulence factor, initiator of inflammation and target for effective immunity. Int. J. Med. Microbiol. *297*, 277–295. https://doi.org/10.1016/J.IJMM.2007.03.012.
47. Moffatt, J.H., Harper, M., Mansell, A., Crane, B., Fitzsimons, T.C., Nation, R.L., Li, J., Adler, B., and Boyce, J.D. (2013). Lipopolysaccharide-deficient Acinetobacter baumannii shows altered signaling through host Toll-like receptors and increased susceptibility to the host antimicrobial peptide LL-37. Infect. Immun. *81*, 684–689. https://doi.org/10.1128/IAI.01362-12.
48. Suzuki, M.M., Matsumoto, M., Yamamoto, A., Ochiai, M., Horiuchi, Y., Niwa, M., Omi, H., Kobayashi, T., and Takagi, T. (2010). Molecular design of LPS-binding peptides. J. Microbiol. Methods *83*, 153–155. https://doi.org/10.1016/J.MIMET.2010.08.009.
49. Castledine, M., Padfield, D., Sierocinski, P., Soria Pascual, J., Hughes, A., Mäkinen, L., Friman, V.P., Pirnay, J.P., Merabishvili, M., De Vos, D., and Buckling, A. (2022). Parallel evolution of Pseudomonas aeruginosa phage resistance and virulence loss in response to phage treatment in vivo and in vitro. Elife *11*, e73679. https://doi.org/10.7554/ELIFE.73679.
50. Penadés, J.R., Chen, J., Quiles-Puchalt, N., Carpena, N., and Novick, R.P. (2015). Bacteriophage-mediated spread of bacterial virulence genes. Curr. Opin. Microbiol. *23*, 171–178. https://doi.org/10.1016/J.MIB.2014.11.019.
51. Hesse, S., and Adhya, S. (2019). Phage therapy in the twenty-first century: facing the decline of the antibiotic era; is it finally time for the age of the phage? Annu. Rev. Microbiol. *73*, 155–174. https://doi.org/10.1146/ANNUREV-MICRO-090817-062535.
52. Suh, G.A., Lodise, T.P., Tamma, P.D., Knisely, J.M., Alexander, J., Aslam, S., Barton, K.D., Bizzell, E., Totten, K.M.C., Campbell, J.L., et al. (2022). Considerations for the use of phage therapy in clinical practice. Antimicrob. Agents Chemother. *66*, e0207121. https://doi.org/10.1128/AAC.02071-21.
53. Schmalstig, A.A., Freidy, S., Hanafin, P.O., Braunstein, M., and Rao, G.G. (2021). Reapproaching old treatments: considerations for PK/PD studies on phage therapy for bacterial respiratory infections. Clin. Pharmacol. Ther. *109*, 1443–1456. https://doi.org/10.1002/CPT.2214.
54. Peng, H., and Chen, I.A. (2021). Phage engineering and the evolutionary arms race. Curr. Opin. Biotechnol. *68*, 23–29. https://doi.org/10.1016/J.COPBIO.2020.09.009.
55. Lavigne, R., and Loessner, M.J. (2021). Editorial overview: Phage therapy in the 21st century - inspired by biotechnology. Curr. Opin. Biotechnol. *68*. vi–vii. https://doi.org/10.1016/J.COPBIO.2021.04.002.
56. Lenneman, B.R., Fernbach, J., Loessner, M.J., Lu, T.K., and Kilcher, S. (2021). Enhancing phage therapy through synthetic biology and genome engineering. Curr. Opin. Biotechnol. *68*, 151–159. https://doi.org/10.1016/J.COPBIO.2020.11.003.
57. Gordillo Altamirano, F.L., and Barr, J.J. (2021). Unlocking the next generation of phage therapy: the key is in the receptors. Curr. Opin. Biotechnol. *68*, 115–123. https://doi.org/10.1016/J.COPBIO.2020.10.002.
58. Payaslian, F., Gradaschi, V., and Piuri, M. (2021). Genetic manipulation of phages for therapy using BRED. Curr. Opin. Biotechnol. *68*, 8–14. https://doi.org/10.1016/J.COPBIO.2020.09.005.
59. Smith, G.P. (2019). Phage display: simple evolution in a petri dish (Nobel Lecture). Angew. Chem. Int. Ed. Engl. *58*, 14428–14437. https://doi.org/10.1002/ANIE.201908308.
60. Bernard, J.M.L., and Francis, M.B. (2014). Chemical strategies for the covalent modification of filamentous phage. Front. Microbiol. *5*, 734. https://doi.org/10.3389/FMICB.2014.00734.
61. Yang, S.H., Chung, W.J., McFarland, S., and Lee, S.W. (2013). Assembly of bacteriophage into functional materials. Chem. Rec. *13*, 43–59. https://doi.org/10.1002/TCR.201200012.
62. Carpenter, B.L., Feese, E., Sadeghifar, H., Argyropoulos, D.S., and Ghiladi, R.A. (2012). Porphyrin-cellulose nanocrystals: a photobactericidal material that exhibits broad spectrum antimicrobial activity. Photochem. Photobiol. *88*, 527–536. https://doi.org/10.1111/J.1751-1097.2012.01117.X.
63. Nakonieczna, J., Wolnikowska, K., Ogonowska, P., Neubauer, D., Bernat, A., and Kamysz, W. (2018). Rose Bengal-mediated photoinactivation of multidrug resistant Pseudomonas aeruginosa is enhanced in the presence of antimicrobial peptides. Front. Microbiol. *9*, 1949. https://doi.org/10.3389/FMICB.2018.01949.
64. Nakonieczna, J., Wozniak, A., Pieranski, M., Rapacka-Zdonczyk, A., Ogonowska, P., and Grinholc, M. (2019). Photoinactivation of ESKAPE pathogens: overview of novel therapeutic strategy. Future Med. Chem. *11*, 443–461. https://doi.org/10.4155/FMC-2018-0329.
65. Malik, Z., Ladan, H., and Nitzan, Y. (1992). Photodynamic inactivation of Gram-negative bacteria: Problems and possible solutions. J. Photochem. Photobiol., B *14*, 262–266. https://doi.org/10.1016/1011-1344(92)85104-3.
66. Ngo-Duc, T.T., Alibay, Z., Plank, J.M., Cheeney, J.E., and Haberer, E.D. (2020). Gold-decorated M13 I-forms and S-forms for targeted photothermal lysis of bacteria. ACS Appl. Mater. Interfaces *12*, 126–134. https://doi.org/10.1021/ACSAMI.9B15682.
67. Ray, P.C., Khan, S.A., Singh, A.K., Senapati, D., and Fan, Z. (2012). Nanomaterials for targeted detection and photothermal killing of bacteria. Chem. Soc. Rev. *41*, 3193–3209. https://doi.org/10.1039/C2CS15340H.
68. Costantini, P.E., Di Giosia, M., Ulfo, L., Petrosino, A., Saporetti, R., Fimognari, C., Pompa, P.P., Danielli, A., Turrini, E., Boselli, L., and Calvaresi, M. (2021). Spiky gold nanoparticles for the photothermal eradication of colon cancer cells. Nanomaterials *11*, 1608. https://doi.org/10.3390/NANO11061608.
69. Peng, H., Rossetto, D., Mansy, S.S., Jordan, M.C., Roos, K.P., and Chen, I.A. (2022). Treatment of wound infections in a mouse model using Zn2+-releasing phage bound to gold nanorods. ACS Nano *16*, 4756–4774. https://doi.org/10.1021/acsnano.2c00048.
70. Koskella, B., and Meaden, S. (2013). Understanding bacteriophage specificity in natural microbial communities. Viruses *5*, 806–823. https://doi.org/10.3390/V5030806.
71. Kömerik, N., Wilson, M., and Poole, S. (2000). The effect of photodynamic action on two virulence factors of Gram-negative bacteria. Photochem. Photobiol. *72*, 676–680. https://doi.org/10.1562/0031-8655(2000)072<0676:teopao>2.0.co;2.

72. Giuliani, F., Martinelli, M., Cocchi, A., Arbia, D., Fantetti, L., and Roncucci, G. (2010). In vitro resistance selection studies of RLP068/Cl, a new Zn(II) phthalocyanine suitable for antimicrobial photodynamic therapy. Antimicrob. Agents Chemother. *54*, 637–642. https://doi.org/10.1128/AAC.00603-09.
73. Rapacka-Zdonczyk, A., Wozniak, A., Pieranski, M., Woziwodzka, A., Bielawski, K.P., and Grinholc, M. (2019). Development of Staphylococcus aureus tolerance to antimicrobial photodynamic inactivation and antimicrobial blue light upon sub-lethal treatment. Sci. Rep. *9*, 9423–9518. https://doi.org/10.1038/s41598-019-45962-x.
74. Tomb, R.M., Maclean, M., Coia, J.E., MacGregor, S.J., and Anderson, J.G. (2017). Assessment of the potential for resistance to antimicrobial violet-blue light in Staphylococcus aureus. Antimicrob. Resist. Infect. Control *6*, 100–113. https://doi.org/10.1186/s13756-017-0261-5.
75. Nikinmaa, S., Podonyi, A., Raivio, P., Meurman, J., Sorsa, T., Rantala, J., Kankuri, E., Tauriainen, T., and Pätilä, T. (2021). Daily administered dual-light photodynamic therapy provides a sustained antibacterial effect on Staphylococcus aureus. Antibiotics *10*, 1240. https://doi.org/10.3390/ANTIBIOTICS10101240.
76. Moore, C.M., Pendse, D., and Emberton, M. (2009). Photodynamic therapy for prostate cancer-a review of current status and future promise. Nat. Clin. Pract. Urol. *6*, 18–30. https://doi.org/10.1038/NCPURO1274.
77. Hamblin, M.R., and Abrahamse, H. (2021). Factors affecting photodynamic therapy and anti-tumor immune response. Anti Cancer Agents Med. Chem. *21*, 123–136. https://doi.org/10.2174/1871520620666200318101037.
78. Henderson, T.A., and Morries, L.D. (2015). Near-infrared photonic energy penetration: can infrared phototherapy effectively reach the human brain? Neuropsychiatric Dis. Treat. *11*, 2191–2208. https://doi.org/10.2147/NDT.S78182.
79. Vanerio, N., Stijnen, M., De Mol, B.A.J.M., and Kock, L.M. (2019). Biomedical applications of photo- and sono-activated Rose Bengal: a review. Photobiomodul. Photomed. Laser Surg. *37*, 383–394. https://doi.org/10.1089/PHOTOB.2018.4604.
80. Qian, X., Zheng, Y., and Chen, Y. (2016). Micro/Nanoparticle-augmented Sonodynamic Therapy (SDT): breaking the depth shallow of photoactivation. Adv. Mater. *28*, 8097–8129. https://doi.org/10.1002/ADMA.201602012.
81. Costley, D., Nesbitt, H., Ternan, N., Dooley, J., Huang, Y.Y., Hamblin, M.R., McHale, A.P., and Callan, J.F. (2017). Sonodynamic inactivation of Gram-positive and Gram-negative bacteria using a Rose Bengal-antimicrobial peptide conjugate. Int. J. Antimicrob. Agents *49*, 31–36. https://doi.org/10.1016/J.IJANTIMICAG.2016.09.034.
82. Brossard, K.A., and Campagnari, A.A. (2012). The Acinetobacter baumannii biofilm-associated protein plays a role in adherence to human epithelial cells. Infect. Immun. *80*, 228–233. https://doi.org/10.1128/IAI.05913-11.
83. Garapati, C., Boddu, S.H., Jacob, S., Ranch, K.M., Patel, C., Babu, R.J., Tiwari, A.K., and Yasin, H. (2023). Photodynamic therapy: A special emphasis on nanocarrier-mediated delivery of photosensitizers in antimicrobial therapy. Arab. J. Chem. *16*, 104583. https://doi.org/10.1016/J.ARABJC.2023.104583.
84. Polat, E., and Kang, K. (2021). Natural photosensitizers in antimicrobial photodynamic therapy. Biomedicines *9*, 584. https://doi.org/10.3390/BIOMEDICINES9060584.
85. Abrahamse, H., and Hamblin, M.R. (2016). New photosensitizers for photodynamic therapy. Biochem. J. *473*, 347–364. https://doi.org/10.1042/BJ20150942.
86. Andris-Widhopf, J., Rader, C., Steinberger, P., Fuller, R., and Barbas, C.F. (2000). Methods for the generation of chicken monoclonal antibody fragments by phage display. J. Immunol. Methods *242*, 159–181. https://doi.org/10.1016/S0022-1759(00)00221-0.
87. Passaretti, P., Khan, I., Dafforn, T.R., and Goldberg Oppenheimer, P. (2020). Improvements in the production of purified M13 bacteriophage bio-nanoparticle. Sci. Rep. *10*, 18538–18539. https://doi.org/10.1038/s41598-020-75205-3.
88. Sampaolese, B., Bergia, A., Scipioni, A., Zuccheri, G., Savino, M., Samorì, B., and De Santis, P. (2002). Recognition of the DNA sequence by an inorganic crystal surface. Proc. Natl. Acad. Sci. USA *99*, 13566–13570. https://doi.org/10.1073/PNAS.202471699.
89. Zuccheri, G., Scipioni, A., Cavaliere, V., Gargiulo, G., De Santis, P., and Samorì, B. (2001). Mapping the intrinsic curvature and flexibility along the DNA chain. Proc. Natl. Acad. Sci. USA *98*, 3074–3079. https://doi.org/10.1073/PNAS.051631198.
90. Redmond, R.W., and Gamlin, J.N. (1999). A Compilation of Singlet Oxygen Yields from Biologically Relevant Molecules. Photochem. Photobiol. *70*, 391–475. https://doi.org/10.1111/J.1751-1097.1999.TB08240.X.
91. Bochner, B.R., Gadzinski, P., and Panomitros, E. (2001). Phenotype Microarrays for high-throughput phenotypic testing and assay of gene function. Genome Res. *11*, 1246–1255. https://doi.org/10.1101/gr.186501.

STAR★METHODS

KEY RESOURCES TABLE

REAGENT or RESOURCE	SOURCE	IDENTIFIER
Antibodies		
Anti-M13 g3p monoclonal antibody	New England BioLabs	Cat#E8033; RRID:AB_1559734
HRP-conjugated IgG goat anti-mouse IgG	Jackson	Cat#115-035-166; RRID:AB_2338511
Bacterial and virus strains		
E. coli Tg1	DSMZ	6056
E. coli DH5α	DSMZ	6897
Acinetobacter baumannii ATCC 19606	American Type Culture Collection	19606
Pseudomonas aeruginosa PA14	DSMZ	19882
Staphylococcus aureus ATCC 29213	American Type Culture Collection	29213
M13KO7 Helper Phage	New England BioLabs	NO315S
Hyperphage M13 KO7ΔpIII	PROGEN	PRHYPE
Chemicals, peptides, and recombinant proteins		
Rose Bengal (RB)	Merck	330000
EDC	Merck	03450
Tetrazolium Violet	Merck	T0138
NHS	Merck	130672
ABMDMA	Merck	75068
Amplex Red	Merck	90101
HRP	Merck	P6782
Critical commercial assays		
PowerUp™ SYBR™ Green Master Mix for qPCR	Thermo Fisher Scientific	A25742
LIVE/DEAD™ BacLight™ Bacterial Viability Kit	Thermo Fisher Scientific	L7007
Deposited data		
pPK_LPS	This study	GenBank: OQ803482
pPKC20	This study	GenBank: OQ803483
M13KO7Δg3pΔoriF1	This study	GenBank: OQ803484
Plasmids and phagemids		
pComb3XSS	Addgene	63890
pPK_LPS	This study	GenBank: OQ803482
pPK_C20	This study	GenBank: OQ803483
M13KO7Δg3pΔoriF1	This study	GenBank: OQ803484
Oligonucleotides		
Primer: forward amplification C20 (AD251) GTTTTGAGCTCCAGGTGCAG	This study	N/A
Primer: reverse amplification C20 (AD252) GTTTTACTAGTACTAACGGTAACCTGG	This study	N/A
Primer: forward amplification Li005 (AD300) CAAAAACTATTCGAGCTCGATTAGCAGCATTCGTGCGTGCA	This study	N/A
Primer: reverse amplification Li005 (AD301) CTAGTGCACGCACGAATGCTGCTAA TCGAGCTCGAATAGTTTTTGAGCT	This study	N/A

(*Continued on next page*)

Continued

REAGENT or RESOURCE	SOURCE	IDENTIFIER
Primer: forward M13 F1ori (AD046) AGGCTGCACCGGTGCGTCAG	This study	N/A
Primer: reverse M13 F1ori (AD047) ACACCCGCCGCGCTTAATGCG	This study	N/A
Primer: forward qPCR (AD211) TCCGGCCTTGCTAATGGTAA	This study	N/A
Primer: reverse qPCR (AD212) CGCAAAGACACCACGGAATA	This study	N/A
Software and algorithms		
BLAST	https://blast.ncbi.nlm.nih.gov/BlastAlign.cgi	v 2.6.0
MUSCLE	https://www.ebi.ac.uk/Tools/msa/muscle/	v 3.8.31
ImageJ	GitHub	v 1.43t
NanoScope Analysis	Bruker corporation	v 1.80
MATLAB	Mathworks	v 9.7 R2019b
CytExpert	Beckman	v 2.4
FlowJo	BD Biosciences	v 10
Prism	GraphPad	v 10

RESOURCE AVAILABILITY

Lead contact

Further inquiries and request for data, strains and resources should be directed to the lead contact Alberto Danielli, alberto.danielli@unibo.it.

Materials availability

Materials generated in this study are available upon request from the lead contact.

Data and code availability

- Sequences of plasmids and phagemids generated in this study have been deposited to GenBank and are publicly available as of the date of publication. Accession numbers are listed in the key resources table. All the other data reported in this paper will be shared by the lead contact upon request.
- This paper does not report original code.
- Any additional information required to reanalyze the data reported in this paper is available from the lead contact upon request.

EXPERIMENTAL MODEL AND STUDY PARTICIPANT DETAILS

Bacterial strains used in this study are listed in the key resources table. All the bacterial strains used in this study were routinely cultured in solid LB agar plates or LB liquid medium at 37°C.

METHOD DETAILS

Bacterial cultures

Acinetobacter baumannii ATCC 19606, *Pseudomonas aeruginosa PA*14 (clinical isolate), *Escherichia coli* TG1 and *Staphylococcus aureus* ATCC 29213 were routinely cultured in solid LB agar plates or LB liquid medium. *E. coli* TG1 cells transformed with plasmids or phagemids were grown solid or liquid LB supplemented with appropriate antibiotic as described below.

Phagemid cloning and phage preparation

The translational fusion of the anti-*A. baumannii* (C20) nanobody or the LPS-binding peptide at the N-terminus of the minor capsid protein pIII was performed by cloning the coding sequences of interest in pPK3DsbA a modified version of the pComb3XSS phagemid[86] obtained from Addgene (pComb3XSS was a gift from Carlos Barbas - Addgene plasmid # 63890; http://n2t.net/addgene:63890; RRID: Addgene_63890). Briefly, to generate pPK3DsbA, the ompA leader sequence found in the original pComb3XSS vector was replaced with a dsbA leader sequence, while the SacI-SpeI insert encompassing the original light and heavy chain stuffers was replaced by a multiple cloning site (MCS), in frame with the C-terminal domain of the pIII protein. The gene encoding for the anti-BAP nanobody C20[43] was synthesized by

Eurofins Genomics. Amplification of the synthetic C20 gene with oligonucleotides AD0251 (SacI overhang) and AD0252 (SpeI overhang), generated amplicons that were further purified and digested with SacI/SpeI restriction endonucleases (NEB, New England Biolabs). and then purified through PCR clean-up. The LPS binding peptide coding sequence (KNYSSSISSIRAC,[48]) was obtained by annealing of oligonucleotides AD0300 (CAAAAACTATTCGAGCTCGATTAGCAGCATTCGTGCGTGCA) and AD0301 (CTAGTGCACGCACGAATGCTGCTAA TCGAGCTCGAATAGTTTTTGAGCT), resulting in SacI and SpeI overhangs. Both inserts were directionally cloned into the SacI-SpeI linearized pPK3DsbA vector, generating phagemids pPK_LPS (GenBank: OQ803482) and pPK_C20 (GenBank: OQ803483). Positive clones were validated by sequencing of purified the constructs.

Engineered phages ($M13_{Aba}$ and $M13_{Gram-}$) were generated by co-transforming *E. coli* TG1 with pPK_LPS or pPK_C20 phagemids and a Hyperphage helper derivative (ProGen), M13KO7Δg3pΔoriF1 (GenBank: OQ803484), in which the oriF1 was removed by inverse PCR with oligos AD0046 (AGGCTGCACCGGTGCGTCAG) and AD0047 (ACACCCGCCGCGCTTAATGCG) followed by re-ligation of the amplicon. Thereby, uniform virions (about 600 nm in length), packaging only the pPK phagemids containing the f1 ori where produced. Cotransformants were grown for 24 h in LB medium supplemented with Ampicillin (100 mg L−1), Kanamicin (25 mg L−1) and 0.4 mM IPTG to induce expression of the fusion construct. Purification of phage was performed as previously described.[38] Briefly, the bacterial culture was pelleted for 30 min at 12.000g to separate bacterial cells from phages present in the supernatant. PEG 8000 (4% w/v) and NaCl (3% w/v) were added to the supernatant and incubated for 90 min at 4°C. Next, the solution was centrifuged for 15 min at 12.000g to precipitate virions. The phage pellet was then resuspended in PBS 1x and further purified by isoelectric point (IEP) precipitation.[87] Purified phages were finally resuspended in PBS 1x pH 7.4. Phage concentrations were determined by measurement of the absorbance at 269 nm wavelength in a UV-Vis spectrophotometer (extinction coefficient $\varepsilon = 3.84\ cm^2\ mg{-}1$) using a 320 nm wavelength spectrum as baseline.

Transmission electron microscopy (TEM) analysis

A drop of M13 bacteriophages solution ($1x10^{11}$ v/mL) was deposited on an oxygen plasma cleaned TEM grid (formvar-coated copper 200 mesh, Ted Pella, Redding, CA, USA) for 30 s and then removed with filter paper. The negative staining was performed using 1% uranyl acetate, and the TEM analysis was performed using a JEOL JEM 1400 microscope (JEOL, Tokyo, Japan) operating at 120 kV. The TEM micrographs were analyzed by using ImageJ.

AFM analysis of engineered phages

AFM analysis was performed with a Multimode 8 AFM (Bruker, U.S.A.). Aliquots of concentration-adjusted phage solutions diluted PBS buffer were deposited on the freshly-cleaved muscovite mica (Electron Microscopy Sciences, U.S.A.) surface let to absorb for 2 min. The AFM fluid cell was mounted and flowed with a small volume of ultrapure water (milliQ, Millipore, U.S.A.). Images were taken in PeakForce Tapping in liquid using ScanAsyst Fluid+ probes (Bruker, U.S.A.), and processed with NanoScope Analysis software (ver. 1.80) by only flattening the micrographs. The contour space coordinates of hundreds phages were digitized semi-automatically from the micrographs using a custom-developed algorithm implemented in MATLAB (Mathworks, U.S.A.).[88,89]

Immunoblotting

$M13_{Gram-}$ and $M13_{C20\_Nb}$ purified phages at a concentration of 10^{10} pfu μL−1 were resolved using a 12% (w/v) SDS gel and transferred to a PVDF membrane (GVS). After treatment with blocking solution (5% milk in PBS pH 7.4 with 0.05% Tween), the membrane was incubated with Anti-M13 g3p Monoclonal Antibody (New England BioLabs) diluted 1: 5000 in blocking solution for 1 h at room temperature. After three washes in PBS Tween 0.05%, the membrane was incubated with HRP-conjugated IgG anti-mouse secondary antibody (Jackson) diluted 1:10 000 and incubated for 1 h at room temperature. The membrane development was performed using LightWave Plus - ECL HRP reagent (GVS). Images were acquired via ChemiDoc Imaging System (Bio-Rad).

Validation of phage retargeting by qPCR

Engineered or wild type M13 phages were incubated with exponential phase *P. aeruginosa*, *A. baumannii,* and *E. coli* cells (10^6 CFU·mL^{-1}) for 15 min at room temperature under gentle shaking. Unbound phages were removed by centrifugation and washing, twice in PBS. The bacterial pellet containing bound phages was the resuspended in PBS 1x, collected and store at −20°C. Samples were boiled at 98°C for 15 min, to release the viral genome, and then 2 μL were used as template for the qPCR reaction (PowerUp Green Master Mix; ThermoFisher Scientific) using primers AD211 (TCCGGCCTTGCTAATGGTAA) and AD212 (CGCAAAGACACCACGGAATA), annealing to the C-terminal domain of the pIII gene. Commercial M13K07 (NEB) was used as a standard to set the calibration curve.

Bioconjugation and purification of M13-RB, $M13_{Aba}$ and $M13_{Gram-}$ phages

Rose Bengal (RB) (Merck, Cat. No. 330000) was conjugated to the capsomers of the M13, $M13_{Aba}$ and $M13_{Gram-}$ phage vectors by EDC/NHS cross-coupling reaction between the amine groups of M13 capsomers and the activated carboxylic group of RB, as previously reported.[38] A solution 10 mM of RB in DMSO (Merck, Cat. No. 472301) was prepared. The activation of the RB carboxylic group was carried out, under stirring condition, by adding EDC (Merck, Cat. No. 03450) and NHS (Merck, Cat. No. 130672) to the RB solution, with a final concentration of 10 mM and 15 mM, respectively. The solution was incubated for 3 h at 25°C under constant shaking at 700 rpm (ThermoMixer HC, S8012-0000; STARLAB, Hamburg, Germany). 50 μL of the activated RB solution was then mixed with 1 mL of the M13, $M13_{Aba}$ or

$M13_{Gram-}$ phage solution at a concentration of 2.4×10^{13} virions mL^{-1} (40 nM) in PBS, resulting in a final RB concentration of 500 μM. The mixture was incubated overnight at 25°C and 700 rpm. The bioconjugates were purified using a PD-10 Desalting Column (containing 8.3 mL of Sephadex G-25 Medium, Merck, Cat. No. GE17-0851-01) to remove unreacted RB and the byproducts of the crosslinking reaction using PBS as elution solvent.

Singlet oxygen assay

The production of singlet oxygen ($^1O_2$) generated by light irradiation was detected by monitoring the decline of absorbance of 9,10-Anthracenediyl-bis(methylene) dimalonic acid (ABMDMA) (Merck, Cat. No. 75068), at 401 nm, due to the reaction of $^1O_2$ with ABMDMA to give the corresponding endoperoxide. Iso-absorbing solutions of RB, $M13_{Gram-}$-RB, and $M13_{Aba}$-RB were prepared in deuterated PBS (10 mM, pH 7.4, Merck, Cat. No. 151882). 500 μL of each solution, containing a concentration of 15 μM of RB and 25 μM of ABMDMA, were irradiated with a visible light lamp (Valex cold white LED, with an irradiance of 2.4 mW cm^{-2}, measured with the photo-radiometer Delta Ohm LP 471 RAD) and maintained under vigorous stirring. The singlet oxygen quantum yield (φ_Δ) of RB in deuterated PBS is 0.76[90] and was used as a reference to determine the φ_Δ of $M13_{Gram-}$-RB and $M13_{Aba}$-RB using the following equation: $\varphi_\Delta{}^S = k^S/k^R \times \varphi_\Delta{}^R$, where k^S and k^R are the slopes of the photodegradation rate of ABMDMA of the samples ($M13_{Gram-}$-RB and $M13_{Aba}$-RB) and of the reference (RB), and $\varphi_\Delta{}^S$ and $\varphi_\Delta{}^R$ are the singlet oxygen quantum yields of the samples and the reference, respectively.

Peroxides assay

Amplex Red assay was used to quantify the peroxides generated by light irradiation. Amplex Red (Merck, Cat. No. 90101) is a colorless molecule that reacts with peroxides in the presence of horseradish peroxidase (HRP, Merck, Cat. No. P6782) to produce resorufin, a fluorescent product. The concentration of peroxides was determined by measuring the difference in the fluorescence intensity of the irradiated samples and non-irradiated references. A working solution (WS) was prepared by mixing 10 μL of HRP (0.4 mg mL^{-1}) in PBS with 1 mL of Amplex Red (500 μM) in phosphate buffer (50 mM, pH 7.4). Solutions of RB, $M13_{Gram-}$-RB, and $M13_{Aba}$-RB were prepared at concentrations of 0.0 μM, 0.25 μM, 0.5 μM, 1.0 μM, 2.0 μM, and 4.0 μM of RB in a 96-well plate. The sample solutions were irradiated for 45 min with visible light (white LED Valex 30 W lamp, irradiation power density on the cell plate = 20 mW cm^{-2}; measured with the photo-radiometer Delta Ohm LP 471 RAD). After irradiation, 10 μL of WS was added to each well. The solutions were then incubated for 30 min at room temperature in the dark. Three technical replicates were performed for each sample. An identical plate was prepared and kept in the dark. To calculate the concentration of peroxides in the samples from the fluorescence signal, a calibration curve was made using standard solutions of H_2O_2. The fluorescence emission was measured at 590 nm (λ_{ex} = 530 nm) using a EnSpire Multimode plate reader (PerkinElmer).

Validation of phage retargeting by flow cytometry

RB-conjugated phages were incubated with 10^6 exponential phase bacterial cells, with a virion:bacteria ratio of to 100:1, for 15 min at room temperature and under gently shacking. Bacterial cells were centrifuged at 6000g for 10 min and washed twice with PBS, to remove unbound phages, prior to fixation with a solution of paraformaldehyde (PFA) 4% in PBS for 15 min. Fixed cells were centrifuged and washed three times with PBS to remove excess PFA, resuspended in PBS and analyzed with a CytoFLEX S cytofluorimeter (Beckam Coulter). Events present in the gated population (gating performed on forward (FSC) and side (SSC) scatter) were analyzed for the fluorescence in the FL1 channel (emission filter 585/42 nm). At least 10.000 events were recorded for each sample. Results are presented as percentage of fluorescent cells in comparison to the control (untreated bacterial cells). Data analysis was processed using CytExpert (Beckman) and FlowJo.

Antimicrobial PDT assays

The photodynamic effect of RB-phage bioconjugates was assessed on bacteria grown to exponential phase in planktonic culture. Free Rose Bengal was used as a further control to verify the phage vector platform's targeting efficacy. Bacterial cultures were grown to exponential phase (OD_{600} = 0.4–0.7), pelleted twice by centrifugation for 10 min at 5000g and resuspended in PBS, with a target concentration of 10^6 cfu mL^{-1} 50 μL of this suspension was seeded in triplicate together with the phage conjugates in the wells of two 96 well u-bottom plates (Sarstedt), reaching a final volume of 100 μL. Both plates were preincubated in the dark for 15 min under gentle agitation to allow phage-bacteria interaction. Unbound phages were removed by washing twice in PBS. Then, one of the two plates was exposed to white light (white LED Valex 30 W lamp, irradiation power density on the cell plate = 20 mW cm^{-2}; measured with the photo-radiometer Delta Ohm LP 471 RAD) at room temperature, for 45 min. The second plate, representing the negative control, was kept in the dark at room temperature for the same time. After irradiation, bacteria were gently mixed and transferred to fresh growth medium (LB broth, dilution 1:10) in a 96-well flat bottom plate (Sarstedt). Growth rates of live bacteria were then monitored with an EnSpire Multimode plate reader (PerkinElmer), by measuring the increase of absorbance (OD_{600}) every 10 min for 15 h at 37°C in each well. Absorbance OD_{600} values for each time point were averaged and plotted on graphs mirroring the kinetics (recovery) of growth after irradiation. The antimicrobial activity of PDT was inferred by measuring the delay in time (=number of generations) needed to reach the onset of the exponential phase of growth (normalized OD_{600} = 0.125/0.15), relative to the control sample without sensitizer kept in the dark. Bacterial survival rates of the different strains were normalized with respect to light exposure without RB conjugated phages or free RB, therefore considering the different susceptibility of these strains to light. At least three biological replicates were performed for each sample. Live/dead assay was performed on bacterial cells 20 min after aPDT treatment using the commercial LIVE/DEAD BacLight Bacterial Viability Kit (Thermo Fisher Scientific) according to the manufacturer's instructions.

Metabolic activity after aPDT treatment was evaluated as described before.[91] Briefly, immediately after PDT treatment, cultures were diluted 1:2 in LB medium supplemented with 0.02% Tetrazolium violet (Merck) and then incubated for 16 h at 37°C. The reduction of tetrazolium violet by metabolically active bacteria was estimated by measuring the absorbance at 550 nm using the multimode plate reader EnSpire (PerkinElmer).

QUANTIFICATION AND STATISTICAL ANALYSIS

All statistical inference tests were performed by using GraphPad Prism 10. Tests used and corresponding p values are reported along with each result as appropriate.